Chapter 3

Top Physics

3.1 Introduction

The top quark is a state which the Standard Model tells us to expect, and for which the agreement between recent direct observation at the Tevatron [1, 2] and indirect expectation [3] is already impressive. At the same time, the top quark has a mass approximately twice that of the weak bosons, making it the only fermion which decays to a real W, and the only quark without a spectroscopy of hadrons. Is this an accident or is this a clue? Experiment is the way to know, and in this case we find another curiosity: although the physics is at the limits of sensitivity at the present Tevatron, it becomes accessible with relatively modest enhancements to the accelerator and detectors.

In this chapter we describe results from several preliminary studies of the potential for top physics at a high luminosity Tevatron. We do not suppose a particular operating point or detector configuration, but simply specify the physics reach as a function of integrated luminosity, assuming maintenance of detector performance comparable to the planned CDF and DØ upgrades for Tevatron Run 2. We discuss the expectations for three luminosity goals as described in Section 1.2 of this report: the present Run 2 plan of 1-2 fb^{-1}, an aggressive "stretch" of Run 2 to 10 fb^{-1}, and finally, a more ambitious program with asymptotic statistical precision represented by 100 fb^{-1}.

We first concentrate on $t\bar{t}$ production for $m_t \approx 170$ GeV/c^2. After describing detected event yields, we discuss measurement of the $t\bar{t}$ production cross section, the top mass, some features of the Wtb vertex, decay branching ratios, rare decays, and exotic production mechanisms. We then discuss electroweak single top production, the prospect for isolation of the composite and component signals in this process and derivative measurements. Comparison is made with prospects at other facilities, and we conclude with a tabular summary of Tevatron measurements and their precision.

In all this, we believe we are only beginning to specify the catalog of interesting measurements in the top sector, and that this report is best interpreted as a survey of representative *sensitivities* in the broad program of top physics accessible at the Tevatron.

3.2 Event Samples in $t\bar{t}$

Future $t\bar{t}$ event yields at the Tevatron can be inferred with reliable precision by extrapolating from the situation presently understood at CDF and DØ . The standard $t\bar{t}$ selection is based on the expected decay chain $t\bar{t} \rightarrow (W^+b)(W^-\bar{\mathrm{b}})$ and the subsequent decays of the W's into fermion pairs. At least one W is tagged in the mode $W \rightarrow l\,\nu$ by requiring an isolated high E_T lepton (e or μ) and large $\not\!\!E_T$. In the "dilepton" analysis the leptonic decay of the other W is identified with a loose lepton selection; this mode has small backgrounds but small branching fraction of just 4/81. In the "lepton+jets" mode, the second W decays to quark pairs, giving a larger branching fraction of $24/81 \approx 30\%$ (lepton = e or μ). The final state of (lνb)(jjb) is separated from the primary background, W+jets, by requiring a large multiplicity of high E_T jets and also evidence of a B decay, using either secondary vertex identification (SVX) or a tag of the "soft lepton" from $b \rightarrow cl\nu_l X$ (SLT).

3.2.1 Top Event Selection

We discuss the situation as understood with the CDF detector configuration, which we believe applies generically to a hadron collider detector with charged particle tracking in a magnetic field, good lepton identification, and a silicon microstrip detector for identification of secondary vertices.

In this study, dilepton selection starts with a well identified, isolated, 20 GeV lepton and $\not\!\!E_T \geq 20$ GeV, and then demands an additional lepton passing relaxed cuts and two jets with $E_T \geq 10$ GeV. The efficiency of this selection, ϵ_{dil} is approximately 16% for $M_{top} = 170$ GeV/c^2.

The present l+jets selection selection starts from a single well identified lepton and $\not\!\!E_T$ requirement as above, plus the requirement of at least 3 jets with $E_T \geq 15$ GeV and $|\eta| \leq 2.0$. The combined efficiency of this selection in the e and μ modes, ϵ_{l+3j}, is approximately 29% for $M_{top} = 170$ GeV/c^2.

The b-tagging algorithms are then applied to see which jets in these events are candidates for the 2 b jets expected from $t\bar{t}$ decay. The secondary vertex b-tagging efficiency is a function of the intrinsic efficiency of the silicon detector and the tagging algorithm for a well contained b jet, which combine to give $\epsilon_{SVX} = 44\%$. Including also the limited acceptance of the silicon system, the total probability to tag at least one b jet in any top event is 42% [1]. The soft lepton tag has an efficiency of 13% per b jet and 20% per event. Subtracting the small overlap between algorithms gives a total combined b-tagging efficiency of $\epsilon_{t\bar{t}\rightarrow b+X} = 53\%$ per event. The total efficiency for the l+3jets+btag selection is then $\epsilon_{l+3j*b} = \epsilon_{l+3j} \times \epsilon_{t\bar{t}\rightarrow b+X} = 15\%$.

The constrained fit technique presently used in the top mass measurement requires a "completely reconstructable" event, that is, all 4 final state jets consistent with the $t\bar{t}$ decay hypothesis. The present selection requires a fourth jet with $E_T \geq 8.0$ GeV and $|\eta| \leq 2.4$, and is found to have an efficiency before b-tagging of $\epsilon_{l+4j} = 25\%$.

The signal to background ratio is measured to be approximately 5:1 in the dilepton mode. In the secondary vertex analysis, requiring at least one b-tag, this ratio is 3:1 in the

3 jet selection, and 12:1 in the 4 jet selection.

When	b_{jet}^{SVX}	b_{jet}^{SLT}	$\epsilon_{t\bar{t}\to b+X}$	$\epsilon_{t\bar{t}\to 2b+X}$
Run 1b	44%	13%	53%	13%
Run 2	60%	13%	85%	42%

Table 3.1: b-tagging efficiencies at CDF. The probability to tag b in the geometrical acceptance is b_{jet}. Including detector acceptance, the probability for the combined SVX+SLT techniques to tag either or both b's in a 170 GeV/c^2 top event is given in the last 2 columns.

When	ϵ_{dil}	ϵ_{l+3j}	ϵ_{l+4j}	ϵ_{l+3j*b}	ϵ_{l+4j*b}	$\epsilon_{l+4j*2b}$
Run 1b	16%	29%	25%	15%	13%	3.2%
Run 2	23%	35%	30%	29%	25%	13%

Table 3.2: Efficiencies for kinematic and b-tag selection at CDF. The last column is for tagging both b's, the 2 columns before are for tagging *at least* one b.

3.2.2 Future Top Selection

The top event yields described above will be improved in Run II by upgrades to the CDF and DØ detectors. The impact of these upgrades has been analyzed in detail. For the case of CDF the yield of identified top events will be improved as follows:

- **High P_T Charged Lepton Identification.** The ability to find and match tracks to the shower information in the forward regions will extend good charged lepton identification into the region $1.0 \leq |\eta| \leq 2.0$. Monte Carlo studies indicate that this will increase the acceptance for a 20 GeV lepton from 170 GeV/c^2 top by 22% for each $W \to e\nu$ and 16% for each $W \to \mu\nu$ [6]. We assume here that lepton identification in the forward region will be made to work with signal to background ratios comparable to those in the present top analysis. The improvement in efficiency then scales with acceptance, up to 23% for dileptons, 35% for $l+3$ jets, and 30% for $l+4$ jets. Complete muon coverage in the region $1.0 \leq |\eta| \leq 2.0$, such as that at DØ will improve the yield by another 10%.

- **Secondary Vertex b-Tagging.** The improvement here is significant. The addition of the third view (along the beamline) will eliminate a large fraction of mistags, allowing more efficient selection at constant background. The standalone pattern recognition in the silicon + fibers will improve the acceptance for low P_T tracks and dense jets. The efficiency to tag a fiducial B jet from decay of a 170 GeV/c^2 top is expected to approach 60%. The new silicon system will cover the full length of the luminous region, so that all events are taggable, increasing the acceptance by $\approx 50\%$. The standalone

tracking capability of the inner tracker also extends the fiducial acceptance into the region $1.0 \leq |\eta| \leq 2.0$, where 27% of top events have at least 1 b jet. In the end, 97% of all B tracks in all top events are contained in this system [5]. The efficiency to tag at least 1 b jet in a 170 GeV/c^2 top event with a secondary vertex will be $\sim 81\%$.

- **Soft Lepton and Total b-Tag Efficiency** The soft lepton b-tag is a less powerful, but still useful complement to the secondary vertex tag. The extension of lepton identification to the region $1.0 \leq |\eta| \leq 2.0$ will improve the acceptance of the soft lepton tag by $\sim 15\%$ for each B. We assume, as before, that an acceptable signal to background ratio is achievable, and that the efficiency improvement scales with the acceptance gain. As discussed above, the electron coverage will be slightly better than the muon coverage, giving an overall net improvement of $\sim 12\%$ for each b. After subtracting the overlap fraction the combined b-tagging efficiency of the SVX + SLT algorithms is found to be $\sim 65\%$ per b jet from 170 GeV/c^2 top decay. The probability to tag at least 1 b jet in such a top event will be $\sim 85\%$. If the soft lepton tagging is limited to the central region, this probability will be only slightly reduced to $\sim 83\%$.

- **Double b-Tag** The ability to tag *both* b's in a top event will be useful in the mass measurement and other kinematic studies where it is important to suppress combinatoric confusion. With a tagging efficiency of 65% per b jet as above, we expect a double b-tag efficiency of 42%. This is probably an underestimate, since the presence of a single tag has already reduced the backgrounds considerably, and looser criteria can be applied to either identify the second B or "anti-tag" the non-b jets from W decay. We will take $\epsilon_{t\bar{t}\to 2b+X} \sim 42\%$ as the *lower limit* on the double tag efficiency.

Taking the product of the kinematic and b-tag efficiencies yields the Run II top selection efficiencies shown in Table 3.2. The products of branching ratio times efficiencies are shown in Table 3.3. We see that in the case of CDF, the effect of the upgrade will be to double the efficiency for single b-tagged events, and quadruple the efficiency for double b-tags.

These efficiencies are a function of the coverage and effectiveness of lepton identification, silicon tracking, and jet calorimetry, and can be considered typical for a generic collider detector operating with these systems in the region $|\eta| \leq 2.0$. A similar analysis of the DØ upgrade [8] has verified this by producing comparable results. We will assume in what follows that the efficiencies listed above can be maintained at high luminosities by appropriate evolution of detector technologies.

3.2.3 Yields

The calculation of absolute yields requires a cross section for top production at the Run II operating point of $\sqrt{s} = 2.0$ TeV. We use the central value from the resummed next-to-leading-order calculation of Laenen *et al.*, $\sigma_{t\bar{t}} = 6.8$ pb for $m_t = 175$ GeV/c^2 [9]. For comparison, note that the Standard Model value for the same mass at $\sqrt{s} = 1.8$ TeV is $4.95^{+0.7}_{-0.4}$ pb [10], and that the present measurement is consistent, with $\sigma_{t\bar{t}} = 6.8^{+3.6}_{-2.4}$ pb at CDF [1], and $\sigma_{t\bar{t}} = 5.2 \pm 1.8$ pb at DØ [12]. The future yields are shown for benchmark data

sets in Table 3.4. At $m_t = 175$ GeV/c^2 each inverse femtobarn at the Tevatron will produce approximately 600 b-tagged events and approximately 250 double b-tagged, completely reconstructable events.

When	dilepton	l+3j	l+4j	$l + 3j * b$	$l + 4j * b$	$l + 4j * 2b$
Run 1b	0.8%	8.7%	7.5%	4.5%	3.9%	1.0%
Run 2	1.1%	10%	8.9%	8.6%	7.6%	3.8%

Table 3.3: Total efficiency ($B \cdot \epsilon$) for top selection at CDF. The last column is for tagging both b's, the 2 columns before are for tagging *at least* one b.

Mode	1 fb^{-1}	10 fb^{-1}	100 fb^{-1}
produced	6.8K	68K	680K
dilepton	82	820	8.2K
W + 3j	680	6.8K	68.0K
W + 3j $*$ b	584	5.8K	58.4K
W + 4j	605	6.0K	60.5K
W + 4j $*$ b	517	5.2K	51.7K
W + 4j $*$ bb	258	2.6K	25.8K

Table 3.4: Top yields

3.3 Measurement of the Top Quark Mass

The mass of the top quark is a fundamental Standard Model parameter and should be measured as accurately as possible. In addition, the value of m_t appears significantly in radiative corrections which connect the Standard Model parameters, and a global fit combining m_t and other experimental information tests for consistency and predicts unknowns, notably the unknown mass of the Higgs scalar, m_H. If we assume that LEPII and future Tevatron running will yield $\delta m_W = 20$ MeV/c^2, Section 4.2.4 of this report shows that measurement of m_t with a precision of 2 GeV/c^2 will constrain m_H to within 50% of itself. This is interesting in its own right, and also very useful for sharpening direct Higgs searches at future facilities.

We describe below two complementary techniques for measurement of m_t at the Tevatron using the lepton + jets mode and the dilepton mode. Since the control of systematic effects in these measurements benchmarks the precision for much of the top physics program, the discussion is detailed. We estimate the probable precision of each method as a function of luminosity. We conclude with a projection on the ultimate m_t precision at the Tevatron.

3.3.1 Mass Reconstruction in Lepton+Jets Using a Constrained Fit

The most accurate technique at present for top mass measurement at the Tevatron is complete reconstruction in $t\bar{t} \rightarrow$ W + 4 jets [1, 2, 13]. Events are selected according to the prescription described in Sec. 2.1, and the lepton and the four highest E_T jets in the event are fit to the hypothesis $t\bar{t} \rightarrow (Wb)(Wb) \rightarrow (l\nu b)(jjb)$. Each jet is extrapolated back to a parton energy by correcting on average for instrumental effects (e.g. calorimeter nonlinearity) and physics complications (e.g. out of cone radiation, semileptonic B decays). The fit tries all jet-parton assignments, allowing jet energies to vary within the expected resolution, constraining $M(l\nu) = M(jj) = m_W$ and $m_t = M_{\bar{t}}$. The 2-C fit has multiple solutions in each top event due to incorrect assignment of jets to primary partons and the quadratic ambiguity in the longitudinal momentum of the neutrino from $W \rightarrow l\nu$. Solutions are chosen according to low or lowest χ^2 and consistency with b-tagging. The shape of the mass spectra for various values of m_t, as well as that expected for the W+4 jets and other backgrounds, are derived from Monte Carlo samples, and a maximum likelihood fit to the data yields the best estimate of the top mass. The outcome of this procedure in the present analysis is $m_t = 176 \pm 8 \pm 10$ GeV/c^2 at CDF and $m_t = 170 \pm 15 \pm 10$ GeV/c^2 at DØ [1, 14].

3.3.2 Experimental Issues in the Constrained Fit

Almost all of the individual systematic uncertainties in the top mass measurement are coupled to the reliability of the Monte Carlo models for the distribution of fit masses in background and signal. This issue has both theoretical and experimental components. We describe here the experimental issues as presently understood, and return to the theoretical issues later.

The expected mass distribution in top events has been studied with the HERWIG Monte Carlo [15] and the CDF detector simulation. The calorimeter response in this simulation has been tuned to the data in a variety of ways, from single track response to jet balancing in large inclusive samples, and the simulated jet energies are extrapolated back to parton energies using the same prescription employed for real data. The shaded histogram in Fig. 3.1 shows the mass distribution at $m_t = 170$ GeV/c^2 when the MC level information is used to pick the correct final state assignments. The distribution is approximately Gaussian, with mean of 170.0 GeV/c^2 and $\sigma = 11.0$ GeV/c^2.

The instrumental contributions to the jet energy resolution include calorimeter nonlinearity, losses in cracks and dead zones, and absolute energy scale. However, the dominant part of the jet energy uncertainty is related to the reliability of the extrapolation to parton energies, and it is the understanding of QCD, not the detector, which presently limits the mass resolution. Both issues can be addressed by *in situ* calibration procedures which use energy balance in e.g. γ+ jet and (Z $\rightarrow$ ee) + 1 jet events. For the instrumental calibration one constructs an energy and position dependent map of the hadronic response in terms of the well measured electromagnetic one. For the QCD issues one studies energy flow in the jet cone and its comparison to Monte Carlo simulations. The latter has many subtleties: Is the hadronic environment in the control samples applicable to top events? How much does

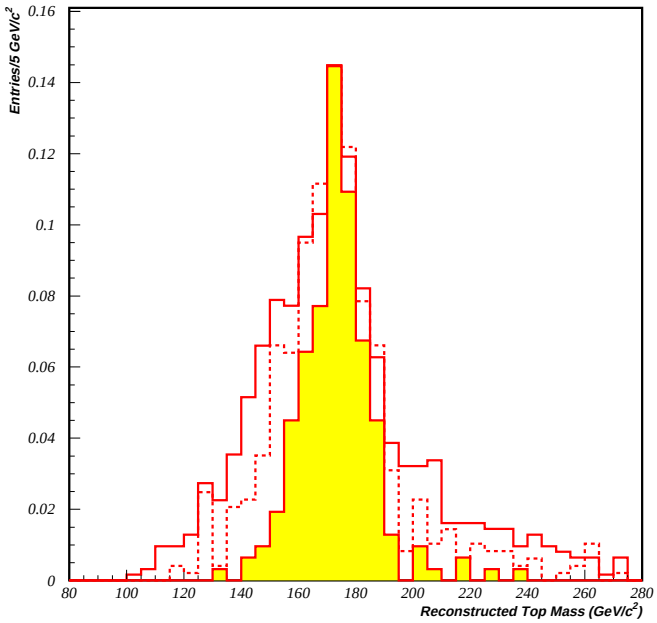

Figure 3.1: The distribution of constrained fit masses for HERWIG $t\bar{t}$ events with $m_t = 170$ GeV/c^2. Shaded curve is correct jet-parton assignment, solid curve is the lowest χ^2 solution with 1 b tagged, dashed curve is with 2 b's tagged.

jet energy tuning depend on parton flavor?

In addition to the jet energy uncertainties, the mass resolution is broadened by combinatoric confusion in the identification of the right parton-jet assignment. The HERWIG model of the procedure suggests that the four jet selection employed here is contaminated by an ISR or FSR initiated jet approximately 50% of the time, and that the minimum χ^2 solution contains an incorrect assignment (above and beyond an ISR/FSR substitution) approximately 40% of the time. All told, the correct 4 jet assignment is ~30% probable. In Fig. 3.1 the mass distribution of the solution with lowest $\chi^2 \leq 10$ and one b-tag is shown as the solid curve. The mean shifts only slightly but the width broadens by 40% to $\sigma = 15$ GeV/c^2. Since the level of combinatoric confusion depends strongly on the population of extra jets and the population of kinematic configurations which give "multiple" solutions, it is again clear that the reliability of the QCD models is the greatest source of systematic uncertainty.

Although the single b-tag requirement reduces the number of possible combinations from 24 to 12, it has little effect on the overall width compared to the case of no b-tagging. The impact of single b-tag is on background control. However the effect of double b-tagging on the combinatoric width is significant. The mass distribution in events with both b's identified is shown as the dashed curve in Fig. 3.1. The double tag restores the width of the

Effect	.07 fb^{-1}	1 fb^{-1}	10 fb^{-1}	comment
Jet scale QCD	7.7	2.0	0.6	$1\sqrt{N}$ scaling
Jet scale calorimetry	3.1	0.8	0.3	$1\sqrt{N}$ scaling
Jet scale total	8.3	2.1	0.7	sum in quad of above
Jet scale total		3.3	1.0	realistic (see 3.4.B)
b-Tagging Bias	2.4	0.6	0.2	control studies
Background Shape	1.6	1.6	0.6	control studies
Fitting Technique	3.1	0	0	
Monte Carlo Stats	3.1	0	0	
Total	10	3.7	1.2	

Table 3.5: Systematic uncertainties in top mass determination. All errors are in GeV/c^2. The first column is based on a preliminary CDF Run 1 result. The extrapolation to higher luminosities is discussed in text

central peak to $\sigma = 12$ GeV/c^2, leaving most of the effect of the combinatoric confusion in modest non-Gaussian tails.

The quantitative relation between the individual uncertainties (i.e. δE^{jet}_{scale}) and the final fit top mass is presently the object of serious study. The size of each uncertainty is estimated from a control sample study, and physics models like HERWIG and VECBOS [16] are used with detector models to propagate the effect through the full simulation including combinatoric confusion. A rule that seems to be emerging is that there is an approximately linear relation between jet energy uncertainties of all kinds and the top mass precision, given by

$$\delta m_t(\mathrm{Gev/c^2}) \approx (1.0) \times \delta E^{jet}_{scale}(\%)$$

The presently understood uncertainties from jet scale ambiguities due to both calorimetry and QCD are shown in the left-most column in Table 3.5, which represents conclusions from an analysis using 67 pb^{-1}at CDF.

Several other sources of uncertainty as understood at present are also listed in the leftmost column of Table 3.5. The size of any potential bias from the b-tagging requirements is studied with B control samples and top Monte Carlo. The reliability of the W+4 jet background model (VECBOS) is verified in the data at low jet multiplicity and a mass uncertainty is derived by studying the fit mass for reasonable variations of the model input parameters. In the present analysis there are small but significant uncertainties due to limited Monte Carlo samples and changes seen with variation of statistical techniques. The sum of all effects at present is estimated to be 10 GeV/c^2.

3.3.3 Future Precision of the Constrained Fit

Early studies have verified that the statistical uncertainty in the constrained fit does scale like $1/\sqrt{N}$ [17]. The HERWIG model studies above can then be normalized to the present

Mode	δm_t	.07 fb^{-1}	1 fb^{-1}	10 fb^{-1}
stat. W+4j	$38/\sqrt{N}$	12	1.6	0.5
stat. W+4j+b	$35/\sqrt{N}$	8	1.5	0.5
stat. W+4j+bb	$27/\sqrt{N}$	25	1.7	0.5
sys. W+4j+b	$43/\sqrt{N}$	10	2.5	0.8
sys. W+4j+b	Table 5	10	3.7	1.2
total W+4j+b	$\delta^2_{stat} + \delta^2_{sys}$	13	4.0	1.3

Table 3.6: Expected precision on the top mass, all entries in GeV/c^2. The statistical errors use the yields from Table 4. The total error is computed using the systematic uncertainties from Table 5.

yields in order to predict future precision. The statistical errors for the three event classes W+4j, W+4j+b, and W+4j+bb are shown in Table 3.6 for the present measurement and the first two luminosity scenarios, where the latter cases assume the event yields outlined in Sec. 2.3. We see that in any of the possible b-tagging modes, the statistical error is well below 1 GeV/c^2 by 10 fb^{-1}.

If the systematic error is linearly related to its component uncertainties, and these uncertainties are measured by mean values in data driven control studies, we expect the systematic uncertainty to also scale as $\approx 1/\sqrt{N}$. This scaling has been observed in CDF W mass results over the Tevatron history, and the measurement of the W mass, like the top mass, is dominated by calorimetric and energy scale uncertainties. If the systematic precision in m_t scales like statistics, the present studies imply the evolution given in the 4th row of Table 3.6.

A slightly more careful accounting of probable evolution of the systematic error is tabulated under the single horizontal line in Table 3.5. The dominant uncertainties due to jet energy scales are discussed in detail below. The b-tag bias can be addressed in control sample studies, and should scale as $1/\sqrt{N}$. Limitations due to the size of Monte Carlo samples and statistical techniques are clearly artifacts of the present immaturity, and we assume that these will go to zero with time. The small but significant uncertainty due to background modelling is a Monte Carlo derived quantity; we assume that progress will become possible when a control sample does, this is discussed below. The net effect of this somewhat more careful consideration of the systematic error is listed at the bottom of Table 3.5 and in the fifth row of Table 3.6, and is seen to be only slightly degraded from simple $1/\sqrt{N}$ scaling.

Adding in quadrature the more conservative of the systematic errors with the statistical error leads to the top mass precision listed at the bottom of Table 3.6. With 10 fb^{-1} at the Tevatron, the experimental contributions to the top mass uncertainty will be limited to the order of 1.3 GeV/c^2 per experiment.

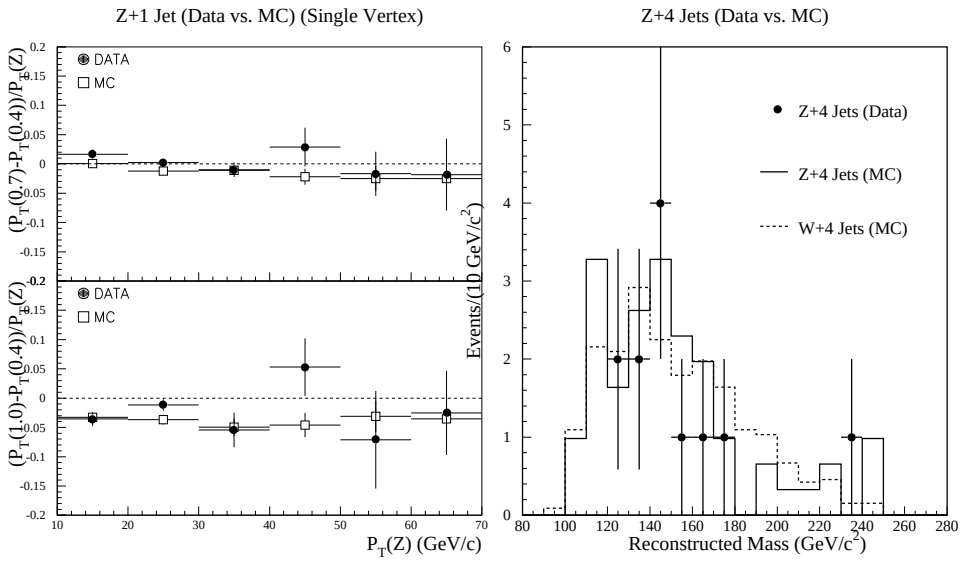

Figure 3.2: The left plot shows calibration of QCD jets in Z + 1 jet events. The right-hand plot shows calibration of background models with Z+4 jets in the Run 1B CDF data.

3.3.4 Elaborations on Future Precision of the Constrained Fit

The systematic uncertainty on m_t will scale as $1/\sqrt{N}$ until the precision is good enough to resolve problems that are *not* amenable to calibration in the data set. We have considered a number of issues and approaches, which, although not exhaustive, suggest that large data sets will provide ample opportunities for the control of systematic effects.

A. Calibration of Jet Scale Using ($Z \to e^+e^-$) + 1 Jet Events

Jet balance studies using γ+jet events are compounded by photon backgrounds and fragmentation complications; as large statistics become available, Z+1 jet events will be sample of choice for this technique. The Z P_T is assumed to measure the P_T of the recoil jet, which can then be compared to simulation to study instrumental scales, soft final state radiation, etc. A model study of the latter [18] is summarized in Fig. 3.2. The energy flow around the jet or parton is quantified in terms of energy in the annulus of, e.g. $\Delta R = 1.0 - 0.4$, and a comparison is made between data and Monte Carlo as a function of jet P_T. It is of interest to note that the effect of multiple interactions on the measured jet energies is included in this study.

The present CDF analysis has used 10% for the uncertainty represented here, leading to the 7.7 GeV uncertainty for the Run 1B "Jet scale QCD" in Table 3.5. Fig. 3.2 suggests that this is an overestimate. In addition, we may imagine that a study of this kind can be used to *tune* the Monte Carlo response model, in which case there would be a bin-by-bin correction to the Monte Carlo jet energies, with precision then limited by the statistical error on the data points in Fig. 3.2. If such a tuning works, then, assuming a conservative value of 3% for the statistical error in Fig. 3.2, and a transfer function $\delta m_t(\mathrm{GeV/c^2}) = 1.0 \times \delta E^{jet}_{scale}(\%)$, the jet scale error would decrease to ≈ 1 GeV/c^2 at 1 fb^{-1}and 0.3 GeV/c^2 at 10 fb^{-1}. A similar treatment of the absolute energy scale reaches the same precision.

With very good resolution it may become clear that there are differences in the details of jets in Z+jets and top events, and scaling the precision from this technique will break down. For instance B jets may require a different calibration, or the cleanliness of the events

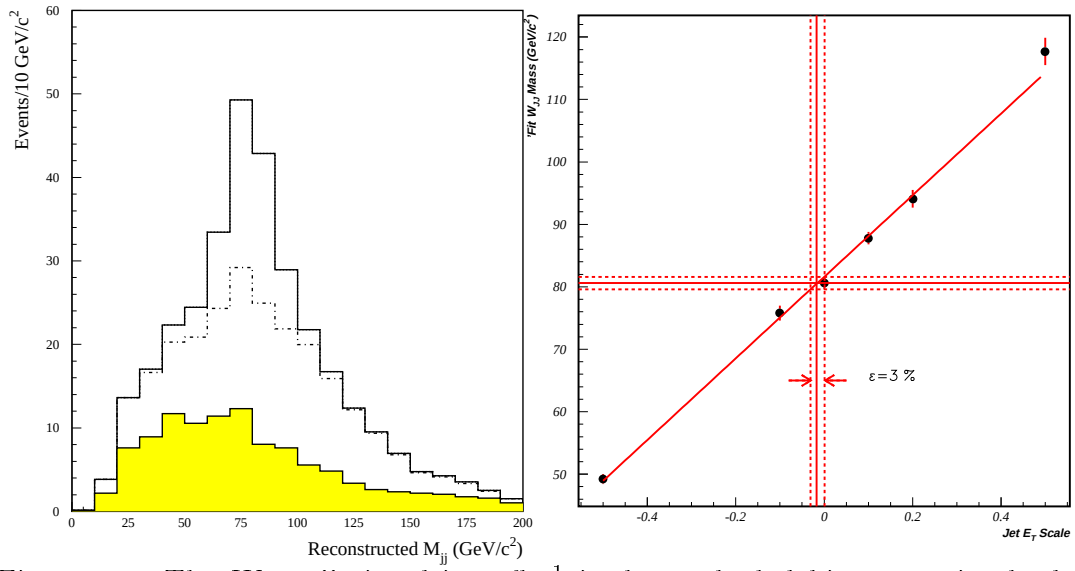

Figure 3.3: The W $\rightarrow$ jj signal in 1 fb^{-1} is the unshaded histogram in the left plot. The shaded curve is the QCD background. The dashed histogram is the QCD background plus the combinatoric background in top events. The excess in the W mass region is 103 events. The right hand plot shows the precision $\delta E^{jet}_{scale}(\%)$ vs $\delta M(jj)$ expected for 1 fb^{-1}.

may have a discernable effect. In this case, *in situ* calibrations, such as the study of light quark jets from W $\rightarrow$ jj as described below will be crucial; however, the statistics and ease of interpretation in the Z+jets sample will continue to make it an essential part of the jet calibration program.

B. Calibration of Total Jet Scale Using W $\rightarrow$ jj in Top Events

This mode is an *in situ* calibration of the instrumental response to and the QCD modeling of light quark jets. We have studied this technique by using the constrained fitting algorithm with the M(jj) = m_W constraint removed. We use the full CDF calorimeter simulation, and the HERWIG and VECBOS models of signal and background, with the ratio normalized to that presently seen in the CDF data. Fig. 3.3 shows the situation expected with 1 fb^{-1}. The shaded histogram is the misidentified W $\rightarrow$ jj in the W+jet background events which fit to the top hypothesis, the dotted histogram is the sum of this and the combinatoric background in top events, and the solid curve represents the correctly identified excess of 103 W $\rightarrow$ jj decays. The excess can be fit to a Gaussian of width 12 GeV/c^2, and implies an accuracy on the mean W mass, in this sample, of $\sim$ 1.3 GeV/c^2.

The transfer function between $\mathrm{E^{jet}_{scale}}$ and a Gaussian fit to the W mass is studied with HERWIG and the CDF simulation, and found to be well fit by the linear relation displayed on the right in Fig. 3.3. The energy scale precision derived from the W $\rightarrow$ jj signal in 1 fb^{-1} is found to be $\delta\mathrm{E^{jet}_{scale}} \approx 3.0\%$. This calibration procedure will certainly improve as $1/\sqrt{N}$. If it is correct, and there were only light quarks in top decay, the $\mathrm{E^{jet}_{scale}}$ contribution to m_t in 1 and 10 fb^{-1} runs would be as given in the 4th row of Table 3.5, slightly worse than $1/\sqrt{N}$ scaling from the first column, but still rather respectable. Of course, the jets are not all light quarks, there are B jets as well, and this issue is discussed in Section C below.

Another interesting feature of this measurement is the distinguishable combinatoric background to W $\rightarrow$ jj from top events. In events with double b-tag we know, in principle,

which jets should be coming from the W. With sufficient statistics the sidebands on the $W \to jj$ peak will therefore be an indirect calibration of the Monte Carlo model dependence for extra jets in top events and final state kinematics.

C. Calibration of B jet energy scale

There is a significant difference between the calorimeter measurement for B jets and light quark jets: some B jets contain muons and neutrinos from cascade decays, and the measured energies have a low side tail not present in light quark jets. At present the effect on the top mass measurement is modelled using Monte Carlo, but several avenues for systematic studies in control samples have been identified. A preliminary study done at CDF suggests that it is possible to improve the B jet energy scale using double b-tagged dijet events [19], however, the improved statistics of Run 2 will be required for real progress. Good b-tagging and implementation of a secondary vertex trigger may allow isolation of the $Z \to b\bar{b}$ peak, providing a b jet calibration tool similar to the $W \to jj$ method described above. Finally, we note that a great deal of information on the energy flow in b jets already exists in LEP data, and this may be a fruitful topic for a LEP-Fermilab collaboration.

D. Calibration of Backgrounds Using ($Z \to e^+e^-$) + 4 Jet Events

The top mass determination involves subtraction of the W+4 jet background, whose shape is modelled with the VECBOS Monte Carlo, and whose uncertainty is presently estimated by varying the VECBOS inputs. As shown in Fig. 3.2 the mass spectrum of the W+4 jet model is very similar to that found with the Z+4 jet model, which can be tested unambiguously in the data [20]. As an example, note that with the present sample of 12 events in 67 pb^{-1}, the mean mass of the Z+4 jet data distribution is known to a precision of 8 GeV/c^2. With 10 fb^{-1}, the corresponding precision is 0.6 GeV/c^2, and will be a stringent test of the VECBOS model of Z+4 jets and W+4 jets as well.

E. Double b-Tagged Events

Table 3.6 shows that with a large sample the statistical error in the *double tagged* sample becomes comparable to that in the single tagged sample. This is obviously because of the reduced combinatoric confusion and therefore improved resolution, as seen in Fig 3.1. It is probable that this sample will also have a smaller systematic error: the backgrounds will be miniscule, and, as mentioned above, the identifiable $W \to jj$ from top decays will be a laboratory for the study of jet and Monte Carlo modelling. The double tag sample may be the sample of choice for the ultimate top mass analysis, with better control of systematic effects than present studies can anticipate.

3.3.5 Top Mass Measurement in the Dilepton Mode

Dilepton events can provide a measurement of the top quark mass complementary to that obtained from l+jets decays. Any differences derived from the two complementary data samples will provide insight into systematic effects or non-standard physics. The signature of a dilepton event consists of two isolated high-p_T leptons, missing p_T due to the neutrinos,

and two jets from the fragmentation of the b quarks. The measurement of the top quark mass from dilepton decays is particularly challenging due to the presence of the two neutrinos in the final state. In this case, in contrast to l+jets events, the measured particle momenta do not contain sufficient information to uniquely constrain the final state. For a given event, in the absence of sufficient constraints for kinematic fitting, an estimator for the top quark mass is defined using a likelihood method.

We describe here a study of top mass finding in dilepton events using the DØ detector model. Monte Carlo samples have been generated using ISAJET and processed through GEANT to simulate the DØ detector response.

3.3.6 Methodology in the Dilepton Mode

We classify dilepton events into three separate categories depending on the flavor of the charged leptons, ee, $e\mu$, and $\mu\mu$. The current DØ event selection criteria are summarized in Table 3.7 [2].

channel	$p_T(e)[Gev/c]$	$p_T(\mu)[Gev/c]$	$p_T(jet)$[Gev/c]	$\not{p}_T$[Gev/c]	H_T[Gev]
ee	> 20	—	> 15	> 25	> 120
$e\mu$	> 15	> 12	> 15	> 20	> 120
$\mu\mu$	—	> 15	> 15	—	> 100

Table 3.7: Selection criteria for dilepton events.

There are 18 unknowns (6 momentum vectors) that specify completely a dilepton final state. We measure 14 observables; 3 each from $\vec{p}(\ell)$, $\vec{p}(\overline{\ell})$, $\vec{p}(b)$, $\vec{p}(\overline{b})$ and the two components of $\vec{\not{p}}_T = \vec{p}_T(\nu) + \vec{p}_T(\overline{\nu})$.

In addition, there are four constraints on the mass of the W boson and top quarks: $m(\ell\overline{\nu}) = m(\overline{\ell}\nu) = m_W$ and $m(\ell\overline{\nu}\overline{b}) = m(\overline{\ell}\nu b) = m_t$. For each assumed value of the top quark mass, m_t, we can therefore solve for the 18 unknowns. In general there are 0, 2 or 4 possible solutions for the top quark momentum vectors. In the analysis, the two highest p_T jets in the events are assumed to be the b jets. Initial and final state gluon radiation can produce additional jets in the event leading to only 53% correct assignments of b jets for top mass of 140 GeV/c^2. Furthermore, since one does not distinguish between b and $\overline{b}$ jets, there is an additional two-fold ambiguity, doubling the possible number of solutions.

For the purpose of constructing an event likelihood for a particular top quark mass hypothesis, a weight w is assigned to each of these possible solutions. The weight w consists of two factors a) parton distribution functions for the initial partons and b) the energy distribution of the charged leptons produced by the decaying top quark in its rest frame [21, 22]. We sum over the weights w for all solutions. Next, in order to account for the detector resolution effects, we generate a pseudo-event-sample by fluctuating the observed lepton p_T, missing p_T, and jet p_T's within the known resolution functions of the DØ detector.

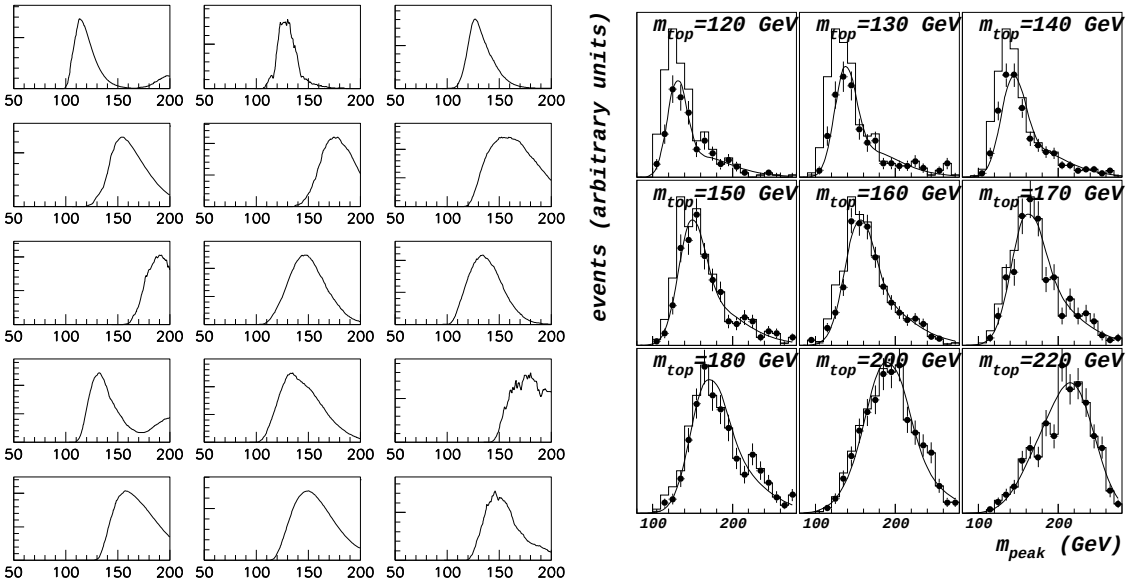

Figure 3.4: Left: Likelihood distributions for fifteen Monte Carlo $t\bar{t} \rightarrow e\mu X$ events with $m_t = 140$ GeV/c^2. Right: Distributions of m_{peak} for Monte Carlo ee events with m_t between 120 and 220 GeV/c^2. The histograms(points) are before(after) the H_T cut and the smooth curves are parametrizations.

The average weight of this pseudo-event-sample is defined as the event likelihood value. This procedure is then repeated for a range of top quark mass hypotheses between 80 GeV/c^2 and 280 GeV/c^2 to get the likelihood curve as a function of top mass for the event [23, 24].

The event likelihood curves for 15 events from a MC sample generated with m_t=140 GeV/c^2 are shown on the left in Fig. 3.4. For each event, we use the peak of this distribution as an estimator of the top quark mass. On the right in Fig. 3.4 we show the distributions of the peak masses for $t\bar{t} \rightarrow ee$ MC samples generated between 120 and 220 GeV/c^2.

3.3.7 Dilepton Mass measurement

To measure the top mass from a sample of events we perform a maximum likelihood fit of the shapes in Fig. 3.4 to the observed peak masses. Figure 3.5 shows the peak masses for five dilepton events in the DØ data sample, the best fit signal shape and the expected background shape. In a preliminary analysis of the DØ dilepton data sample [25], we determine the top quark mass to be

$$m_{top} \;=\; 145 \pm 25 \pm 20 \text{ GeV/c}^2,$$

where the first error is statistical and the second systematic.

3.3.8 Future prospects in the Dilepton Mode

We first consider the statistical error. We generate many pseudo-experiments by selecting samples of MC events. Each of these experiments contain $e\mu$, ee, $\mu\mu$ events distributed in the proportion 2 : 1 : 1, as expected in the SM. We then treat these samples as if they were data and subject them to the same fitting procedure to measure the top quark mass. The rms of the fitted top quark mass per event obtained from 4-event ensembles ranges between

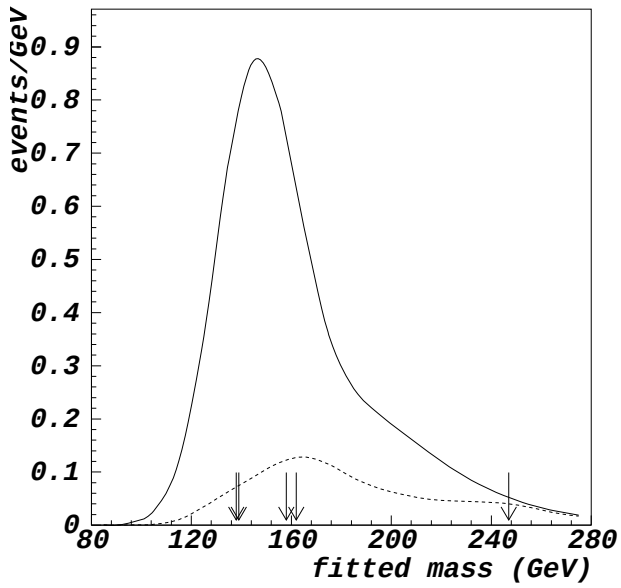

Figure 3.5: Distribution of peak masses for DØ dilepton candidates are shown as arrows. The two curves are the fits for the signal (solid) and the expected background (dashed).

42–56 GeV/c^2 for top masses between 140 and 200 GeV/c^2. Studies for 16-event ensembles show that the statistical precision scales as $\sqrt{\frac{1}{N}}$, and one can easily extrapolate to larger event samples expected with the upgraded Tevatron. The dilepton yields from Table 3.4 are used to calculate the statistical precision of this measurement for various running scenarios. These estimates are shown in the first row in Table 3.8.

At present the major systematic limitations arise from uncertainty about the jet energy scale and the modeling of the gluon radiation in the Monte Carlo generators. The issue of jet energy scale error is an experimental one. The current estimate of this error is 10% which leads to a 7% error in the mass determination. The size of this error depends on the number of Z+jet and W+jet events available to calibrate the jet scale and will therefore decrease as $1/\sqrt{N}$.

Our present understanding of QCD is a limiting factor in the modeling of gluon radiation effects. Uncertainty in the modeling is a large contribution to the systematic error. An estimate of this error is obtained by analyzing samples generated with Monte Carlo event generators which have different underlying models for parton showering and gluon radiation. Using samples of 160 GeV/c^2 $t\bar{t} \rightarrow \ell\ell'$ events generated with three different Monte Carlo models, ISAJET, HERWIG and PYTHIA, we find this error to be 9 GeV/c^2. We also expect this understanding to improve with increased data samples.

Other sources of systematic uncertainty in this measurement have been considered in detail. The estimates of the uncertainties and possible biases due to parametrization of the

likelihood functions, from the finite Monte Carlo statistics available, and our understanding of the signal to background ratio are listed in Table 3.8. The first column lists the errors as understood in the current DØ analysis. These estimates are obtained by reanalyzing a $t\bar{t}$ 160 GeV/c^2 Monte Carlo with changed parameters. The error due to uncertainties in the background normalization will decrease with increasing data samples since the amount of background will be measured more precisely.

Larger dilepton event samples will enable us to utilize the requirement of b-jet tagging for event selection. The double b-jet tagging efficiency of the upgraded detectors is expected to be about 42% (see section 2.2). Even though we lose half the statistics by using this requirement, it reduces the combinatoric confusion in the events. Lower combinatorics will reduce the tails in the peak mass distributions in Fig. 3.4 and lead to lower statistical and systematic errors. Quantitative studies are in progress.

Source	70 pb^{-1}	1 fb^{-1}	10 fb^{-1}
Statistical	25	6.2	2
Jet energy scale	11	2.7	0.9
Event Generator	9	—	—
Background Normalization	4	1	0.3
Monte Carlo Statistics	5	—	—

Table 3.8: Estimates of systematic uncertainties on the top mass measurement from the dilepton mass analysis. All entries are in GeV/c^2.

3.3.9 Conclusions on Dilepton Mass Measurement

With a large top data sample expected from an upgraded Tevatron, the top quark mass measurement in the dilepton channel has good sensitivity as well being a very interesting measurement. While the statistical precision is somewhat less than for the l+jets measurement, it provides an independent measurement of the top quark mass with a data sample that has much less background than the l+jets sample. Moreover, both measurements are likely to be systematically limited with a 10 fb^{-1} data set, so that a second measurement with somewhat different systematics will be valuable.

3.3.10 Ultimate Top Quark Mass Precision at the Tevatron

We have presented two techniques for the measurement of the top mass with precision approaching the order of 1 GeV/c^2 with 10 fb^{-1}. These two initial approaches will certainly be augmented by new ideas and additional techniques. Preliminary studies already suggest the possibility of isolating a signal and making a competitive mass measurement in the 6 jet final state at CDF [26]. In another interesting example, Ref. [27] studies the relation between m_t and the mean b decay length, and suggests that with large statistics the decay

length in the tagged b's, accurately measured in the silicon vertex detectors, could yield an asymptotic statistical precision $\delta m_t \approx 1$ GeV/c^2 . This would give *four* techniques: l+jet, dilepton, all-jet, and decay-length, which are all statistically independent, and for which precise mass values could be combined. Meanwhile, large data sets will provide additional avenues for the study of systematic effects in all cases. We believe that it is reasonable to expect that an integrated data set of 10 fb^{-1} will allow a combined measurement of the top mass with control of the experimental uncertainties at the level of 1 GeV/c^2.

There are additional theoretical complications. For instance, the distribution of fit masses used as input templates to the likelihood fit are ultimately derived from a theoretical calculation, and several studies raise questions concerning the modelling of hard gluon radiation and other subtleties in the final state [28] . Examination of these issues is only beginning, and the final answers will require much more statistical precision than presently available, but we believe it is reasonable to expect that these theoretical uncertainties will ultimately be controlled at the level of the experimental precision, of order 1 GeV/c^2.

Taking all of the above into account, we believe that 10 fb^{-1} at the Tevatron will allow a **measurement of the top mass with a precision of 2 GeV/c^2 per experiment**. This level of precision will challenge the program of precision electroweak measurements. What new measurements should be planned in order to derive maximum benefit from δm_t ~2 GeV/c^2 ? As the electroweak program enters its next decade this will be an interesting question for further study.

3.4 Top Quark Production

The main top production process at the Tevatron is the creation of $t\bar{t}$ pairs through strong $q\bar{q}$ annihilation and gluon fusion. Many models exist for new physics which could modify the rate and final state kinematics of pair production. In addition, electroweak processes can produce a single top quark in association with a b quark, at about 35% of the pair production rate. We discuss below the prospects for measurements and tests with top pair production. Single top physics is discussed in Sec. 6.

3.4.1 Measurement of the $t\bar{t}$ Production Cross Section

An accurate measurement of the $t\bar{t}$ production cross section is a precision test of QCD. A cross section significantly higher than the theoretical expectation would be a sign of non-Standard Model production mechanisms, for example the decay of a heavy resonant state into $t\bar{t}$ pairs [29], or anomalous couplings in QCD [30].

The current measurement of the top production cross section at $\sqrt{s} = 1.8$ TeV, for m_t = 175 GeV/c^2, is $\sigma_{t\bar{t}} = 6.8^{+3.6}_{-2.4}$ pb at CDF and $\sigma_{t\bar{t}} = 5.2 \pm 1.8$ pb at DØ compared to the theoretical value at this mass of $4.95^{+0.7}_{-0.4}$ pb [1, 12, 10].

The uncertainty on the current measurement is dominated by the statistics of the event sample. In the future, systematic uncertainties will be the limiting factor. For the l+jets mode, which dominates the statistics of the measurement, the largest systematic uncertainties are now those on the total acceptance (about 30%), and on the background (about 35%).

The uncertainty on the integrated luminosity is currently about 10%, but will eventually fall to 3.5%, the accuracy of the effective cross section for the luminosity monitor. In Run 2 and beyond, the luminosity will be measured differently, either through the $W \to l\nu$ rate, or the mean number of interactions per crossing. The former is presently understood to 5%, and we will assume this value for the future precision of the luminosity normalization.

	1 fb^{-1}	10 fb^{-1}	100 fb^{-1}
Acceptance	8.4%	2.7%	0.9%
Backgrounds	10%	3.3%	1.0%
Integrated Luminosity	5.0%	5.0%	5.0%

Table 3.9: Assumed systematic uncertainties for the $t\bar{t}$ cross section measurement

Lum	# b-tagged $t\bar{t}$ events	# Background events	Cross section precision
1 fb^{-1}	580	165	11%
10 fb^{-1}	5.8K	1.6K	5.9%
100 fb^{-1}	58K	16K	5.1%

Table 3.10: Precision of $t\bar{t}$ cross section measurement

The systematic uncertainty on the total acceptance is due primarily to three factors: Initial state radiation, jet energy scale, and b-tagging efficiency. Initial state radiation can be studied using a sample of Z+jets, while the jet energy scale uncertainty can be addressed as in the top mass discussion. Both of these techniques are limited in their accuracy by the size of the event sample and so the uncertainties should be substantially reduced in Run II and beyond. The b-tagging efficiency in top events is now measured using a combination of inclusive lepton events and Monte Carlo. The uncertainty is due in part to the comparison between data and Monte Carlo and in part to the size of the inclusive lepton sample. With more than 1 fb^{-1} of data, however, it will be possible to measure the b-tagging efficiency *in top events*, using dilepton events (selected without a b-tag) and the ratio of single to double tags in lepton plus jets events. Thus we expect a significant reduction of the uncertainty on the tagging efficiency in Run II and beyond as well.

The systematic uncertainty on the background estimate for the lepton plus jets mode is dominated by the uncertainty on the heavy flavor content in W+jet events, which is based on Monte Carlo. With sufficient data one can measure the bottom and charm content as a function of jet multiplicity in W + jet events using the $c\tau$ distribution of the tagged jets and use this to tune the Monte Carlo for W + 3 or more jet events, thus significantly reducing the uncertainty.

Lum	Cross section ratio precision
1 fb^{-1}	14%
10 fb^{-1}	4.8%
100 fb^{-1}	1.5%

Table 3.11: Precision of $t\bar{t}$ cross section ratio measurement

It is clear that there are many handles for reducing the systematic uncertainties in the top cross section measurement. In what follows we make the assumption that the systematic uncertainties will decrease according to $1/\sqrt{N}$. Although somewhat arbitrary, this scaling is already observed between the CDF Run 1A vs. Run 1B analyses. We assume that the luminosity uncertainty will increase to 5% . In Table 3.9 we list the expected systematic uncertainties for integrated luminosities of 1, 10 and 100 fb^{-1}.

The background from mis-tags is assumed to drop to zero with three dimensional silicon tracking, and the remainder of the background is assumed to scale both with top acceptance and integrated luminosity. We note that, within reasonable bounds, the cross section uncertainty is rather insensitive to the amount of background for integrated luminosities of 1 fb^{-1} and above. In Table 3.10 we list the expected precision of the $t\bar{t}$ cross section measurement in the l+jets mode for integrated luminosities of 1, 10 and 100 fb^{-1}. With 10 fb^{-1} at the Tevatron it will be possible to measure the total $t\bar{t}$ production rate with a precision of approximately 6%.

3.4.2 The ratio of dilepton to l+jets production rates

The ratio of the $t\bar{t}$ cross section measured using dilepton events to that measured using single lepton plus jets events is also of interest. A value of this ratio significantly different than 1.0 is a signature for non-Standard Model decay modes of the top quark because the acceptances for the two modes are predicated on the assumption of the decay sequence t$\rightarrow W \rightarrow$ leptons. Whereas the measurement of $BF(t \rightarrow b)$ discussed in Section 5.2 is a way to test for top decays without b quarks in the final state, the cross section ratio is primarily aimed at decays without W bosons in the final state, such as charged Higgs t $\rightarrow$ H^+b and light stops t $\rightarrow \tilde{t} + \tilde{\chi}^0$.

To estimate the future precision of the cross section ratio, we again assume the event yields from Table 4. We assume that the luminosity and all acceptance uncertainties, except that due to b-tagging which is not used in the dilepton selection, cancel in the ratio. We assume that the background uncertainties *do not* cancel in the ratio but, as above, that they decrease as $1/\sqrt{N}$ for both channels. For large data sets the uncertainty is simply dominated by the dilepton statistics. In Table 3.11 we list the precision of the measured ratio as a function of integrated luminosity. In section 5.3 we show that with a sample of 10 fb^{-1}, the ratio of the dilepton to l+jets production rates will be sufficient to measure the branching fraction to W in association with b with precision of 3.5%.

3.4.3 Search for $t\bar{t}$ Resonances

Several models have been proposed for extensions of the Standard Model which could produce enhancements or resonances in the $t\bar{t}$ invariant mass ($M_{t\bar{t}}$) spectrum [29, 31]. A color-octet vector meson associated with a top condensate [32] and multiscale technicolor[33] are two examples of phenomena that can enhance $t\bar{t}$ production. In certain theoretical models, the branching fraction of $X \to t\bar{t}$ is large. For example, a topcolor Z′ has a branching fraction to $t\bar{t}$ of 50-80% depending on the Z′ width [34]. It is important to search for heavy objects decaying to $t\bar{t}$ pairs since it may be difficult to observe the resonance in other decay channels. Although alternative techniques have been proposed [31], for this study we directly search for a resonance (a peak) in the $M_{t\bar{t}}$ distribution.

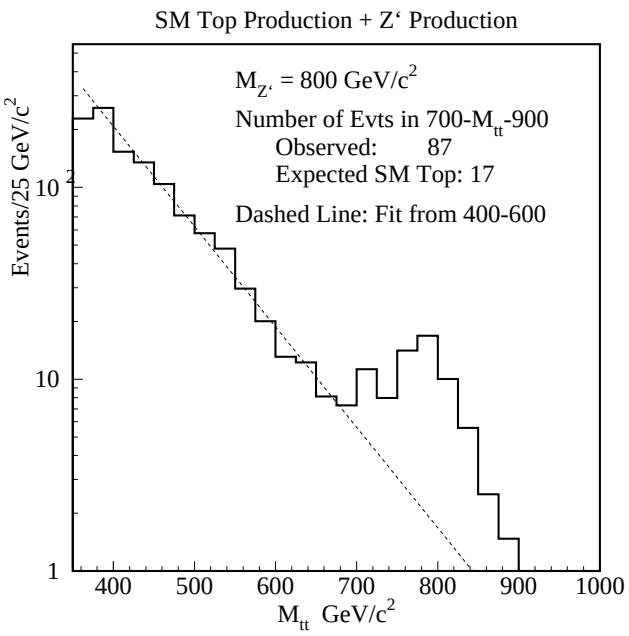

Figure 3.6: A hypothetical $M_{t\bar{t}}$ spectrum with an 800 GeV/c^2 Z′ topcolor boson. The rate is based on the theoretical predicted cross section for $t\bar{t}$ production and Z′ production [34] with 2 fb^{-1}. The standard model prediction (17) in the region 700-900 GeV/c^2 is estimated from the fit. The Z′ results in an addition 70 events in the high mass region.

We reconstruct $M_{t\bar{t}}$ on an event-by-event basis using the same event sample and constrained fitting techniques used in the top mass measurement (see Section 3). We want the best $M_{t\bar{t}}$ resolution possible and therefore we use an additional constraint that the t and $\bar{t}$ decay products have a mass equal to the measured M_{top}. This improves the resolution on $M_{t\bar{t}}$ by a factor of two [35]. Systematic studies show that constraining to an incorrect M_{top} shifts the peak position of the resonance but does not greatly affect the mass resolution. The shift in $M_{t\bar{t}}$, $\Delta M_{t\bar{t}}$, is about twice the shift in M_{top}, $(M_{top}^{true} - M_{top}^{constrained})$. Since M_{top} will be precisely measured, the effect on a resonance peak position will be very small.

For definiteness, we use the example of a topcolor Z′ decaying to a $t\bar{t}$ pair. The cross section, $\sigma \cdot B(X \to t\bar{t})$, is determined by theory. We use the PYTHIA Monte Carlo to provide the decay $X \to t\bar{t}$ and calculate the acceptance. The acceptance is 6.5% and approximately

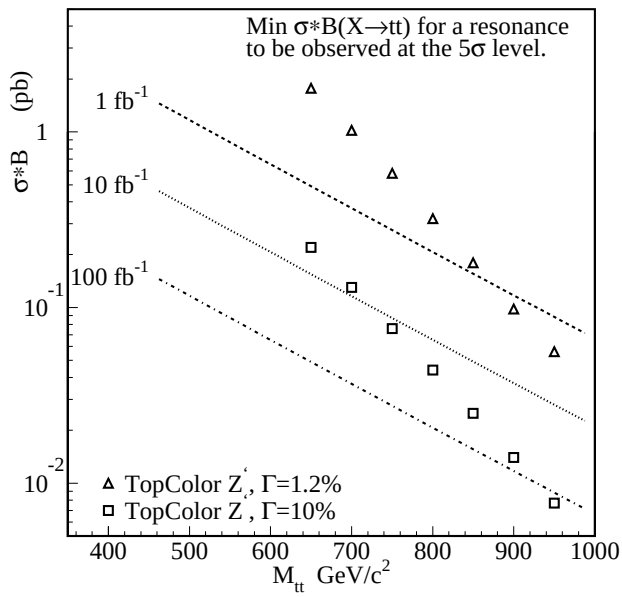

Figure 3.7: $\sigma \cdot B(X \to t\bar{t})$ vs $M_{t\bar{t}}$, where the lines represent the minimum $\sigma \cdot B$ to observe a 5σ excess of events in a sample with 1, 10, and 100 fb^{-1} of integrated luminosity. The triangles (squares) show the $\sigma \cdot B$ for a topcolor Z' with width $\Gamma = 1.2\%$ (10%)[34, 36].

flat versus $M_{t\bar{t}}$. This acceptance includes the branching fractions ($W \to \ell\nu$, $W \to jj$), lepton and jet selection, at least one b-tagged jet, and the reconstruction efficiency of the constrained fitting technique. As a simple example, we add the $M_{t\bar{t}}$ distribution for a Z$'$ ($M_{Z'}$ = 800 GeV/c^2, $\Gamma_{Z'} = 1.2\%$) to the $M_{t\bar{t}}$ distribution from standard model $t\bar{t}$ production. The result is shown in Figure 3.6. A clear resonance can be seen near 800 GeV/c^2. A simple quantification of the excess can be determined by fitting the $M_{t\bar{t}}$ distribution below the resonance to estimate the background in the region 700-900 GeV/c^2. The estimate yields 17 events. With the Z$'$, a total of 87 events are expected in the same region. This excess is well above the 5σ level. More sophisticated methods, involving fitting to standard model and $X \to t\bar{t}$ $M_{t\bar{t}}$ distributions, are being developed to extract an excess of events due to a resonance [35].

We generalize this procedure to determine the minimum $\sigma \cdot B(X \to t\bar{t})$ for a process $X \to t\bar{t}$ to yield a $\geq 5\sigma$ excess of events. For this study we assume the natural width of the object is less than the detector resolution on $M_{t\bar{t}}$ ($\approx 6\%$ at $M_{t\bar{t}}$ = 800 GeV/c^2). If the resonance is wider it can still be observed; however, it simply requires a larger data sample. Figure 3.7 shows the minimum $\sigma \cdot B(X \to t\bar{t})$ for the production of $X \to t\bar{t}$ in order to observe a $\geq$5 sigma excess. The three lines show the results for 1, 10, and 100 fb^{-1} of data. If a theoretical model has a $\sigma \cdot B$ above a line, that object could be observed at a $\geq 5\sigma$ level for the given luminosity. For comparison, the theoretical expectation for a topcolor Z$'$ and Γ = 1.2% (10%) is show by the triangles (squares) [36]. The comparison of the 5σ lines with the $\Gamma_{Z'} = 10\%$ values (squares) is slightly optimistic since $\Gamma_{Z'}$ is larger than the experimental resolution. However, it does represent the approximate reach for these wide resonances. With 10 fb^{-1}, we will be able to observe a narrow Z' resonance out to approximately 800 GeV. A 100 fb^{-1} sample of $t\bar{t}$ events will provide an excellent mass reach for the search for

new phenomena and will test a wide variety of theoretical models.

3.5 Top Quark Decays

In the Standard Model with three generations, existing experimental constraints and the unitarity of the CKM matrix require $|V_{tb}| \simeq 1$, predicting that the weak decay of the top will proceed almost exclusively through W + b. The $t \to Wb$ decay vertex is completely fixed by the universal V – A coupling to the SU(2) bosons. The decay width is given by [37]

$$\Gamma(t \to bW^+) = \frac{G_F m_t^3}{8\sqrt{2}\pi}|V_{tb}|^2[1 - \frac{m_W^2}{m_t^2}]^2[1 + 2\frac{m_W^2}{m_t^2}]$$

For $m_t = 175$ GeV/c^2, this partial (almost total!) decay width is ~ 1.8 GeV, corresponding to a lifetime of $\sim 0.4 \times 10^{-24}$ seconds. This rapid decay cuts off the long distance part of the strong interaction; there is no hadronization, and all strong interaction issues for the top quark should be well described by perturbative QCD. The top quark provides the first opportunity to study the decays of a naked quark, with experimental techniques and advantages familiar from muon decay.

We describe measurements of the decay couplings, branching fractions, rare decays, and a limit on $|V_{tb}|$. The measurement of the decay width, which involves all of these things, is possible through the electroweak production of $t\bar{b}$ pairs, and is discussed in Section 6.

3.5.1 The Structure of the Wtb Vertex

Because the top is heavy, it is possible that the physics of an underlying theory at a high mass scale may manifest itself via new non-universal top interactions. [38]. Very few constraints exist on these parameters from low energy data. A recent analysis of the CLEO $b \to s\gamma$ result [40] suggests that V+A couplings should be small. A recent analysis of LEP results [42] succeeds in limiting only neutral current couplings of the top.

In the case of direct measurements at the top, nature provides a tool which does not exist for the light quarks: a two body weak decay which precedes hadronization and therefore carries helicity information related to the fundamental couplings. In the Standard Model, there are three important conclusions [39]:

- A top decays only to left-handed or longitudinal W's. The longitudinal component of the W is an item of some interest in the Standard Model.
- The ratio of longitudinal to left-handed W's in top decay is given in the Standard Model as

$$\frac{W_{long}}{W_{left}} = \frac{1}{2}(\frac{m_t}{m_W})^2$$

  which is 2.23 for $m_t = 170$ GeV/c^2. Alternatively, we may say that in the Standard Model the branching fraction of the top to longitudinal bosons is an exact prediction

depending only on the top mass, and for e.g. $m_t = 170$ GeV/c^2 we expect to find

$$B(t \to bW_{long}) = \frac{\frac{m_t^2}{2m_W^2}}{1 + \frac{m_t^2}{2m_W^2}} = 69.2\%$$

- Non-universal top couplings will, in many cases, appear as a departure of $B(t \to bW_{long})$ from the value expected for the measured m_t.

The polarization state of the decay W is experimentally accessible through the charged lepton helicity angle, $\cos\theta_e^*$, which is conveniently measured in the lab frame [39] as

$$\cos\theta_e^* \approx \frac{2m_{eb}^2}{m_{eb\nu}^2 - m_W^2} - 1.$$

The resulting $\cos\theta_e^*$ distribution can then be fit to the superposition of W helicity amplitudes to measure $B(t \to bW_{long})$ or, more generally, to measure any possible contribution of non-universal weak couplings in top decay. A method employing the neutrino from W decay to analyse the top couplings is discussed in Ref. [41]

We study the expected sensitivities at the Tevatron using the charged lepton helicity angle technique. We use a four vector level Monte Carlo employing a general chiral Lagrangian treatment of the Wtb vertex and maintaining full helicity information in top decay [42]. For the Standard Model couplings, the unbiased distribution of $\cos\theta_e^*$, constructed as above, using 129K generated events at $m_t = 170$ GeV/c^2, is shown in Fig. 3.8. Superposed on the expected distribution are the two anticipated individual contributions for $m_t = 170$ GeV/c^2

$$\begin{aligned} \frac{dN}{d(\cos\theta_e^*)} &= 0.31 \mid M(W_{left}) \mid^2 + 0.69 \mid M(W_{long}) \mid^2 \\ &= 0.31 \times \frac{1}{4}(1 - \cos\theta_e^*)^2 + 0.69 \times \frac{1}{2}(\sin\theta_e^*)^2 \end{aligned}$$

as well as the sum, which is seen to provide a good fit to the simulation result.

We now consider a CDF/DØ style analysis for $m_t = 170$ GeV/c^2. We assume, to start, that the constrained mass fit will allow us to measure the $\not{E}_T$, the longitudinal component of the neutrino momentum, and all jet energies perfectly, and that we always know which b jet belongs to the semi-leptonic top decay. The effects of smearing all these will be considered below. We impose an event selection similar to the CDF lepton + jets analysis, and use the Monte Carlo to understand how to correct the $\cos\theta_e^*$ distribution for the bias imposed by these cuts. This acceptance corrected distribution for 1000 events is shown as the points on the right in Fig. 3.8. The uncertainties are computed bin by bin and include the uncertainty in the bias correction. We fit the distribution in Fig. 3.8 to the Standard Model hypothesis and get a good fit with $B(t \to bW_{long}) = 0.708 \pm 0.030$, as shown.

We conclude that in the case given here, a sample of 1000 tagged top events will allow the measurement of $B(t \to bW_{long})$ with a statistical precision of roughly 3%. With some confidence in our Monte Carlo tools, we then perform this analysis on a variety of sample sizes, to determine the statistical error as a function of the number of events. The result is

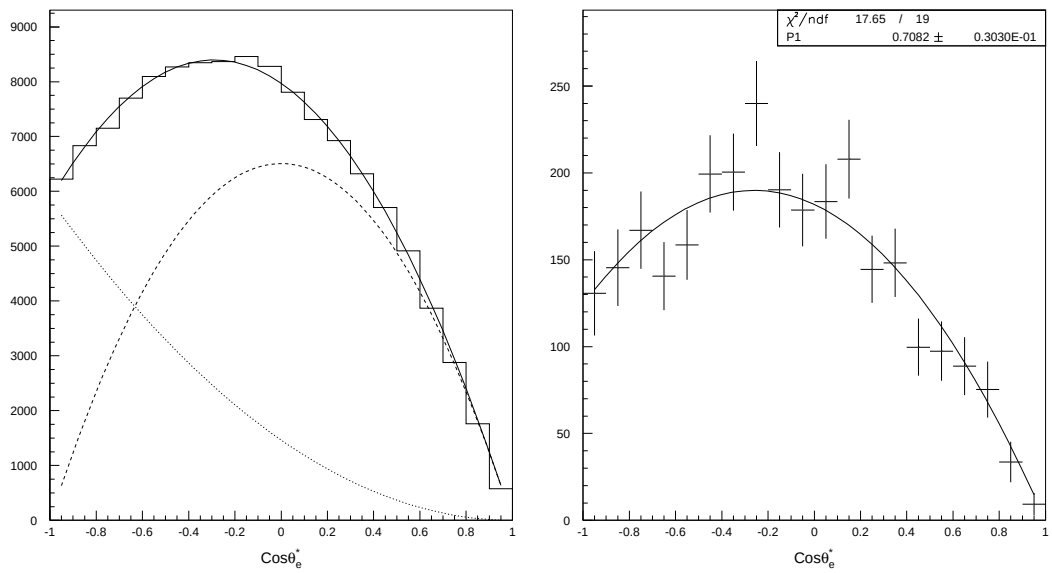

Figure 3.8: Left: The $\cos\theta_e^*$ distribution with perfect reconstruction fitted to the sum (solid) expected contributions from W_{left} (dot) and W_{long} (dash) in the Standard Model. Right: The $\cos\theta_e^*$ distribution for 1000 events (points with errors) and fit to the Standard Model hypothesis.

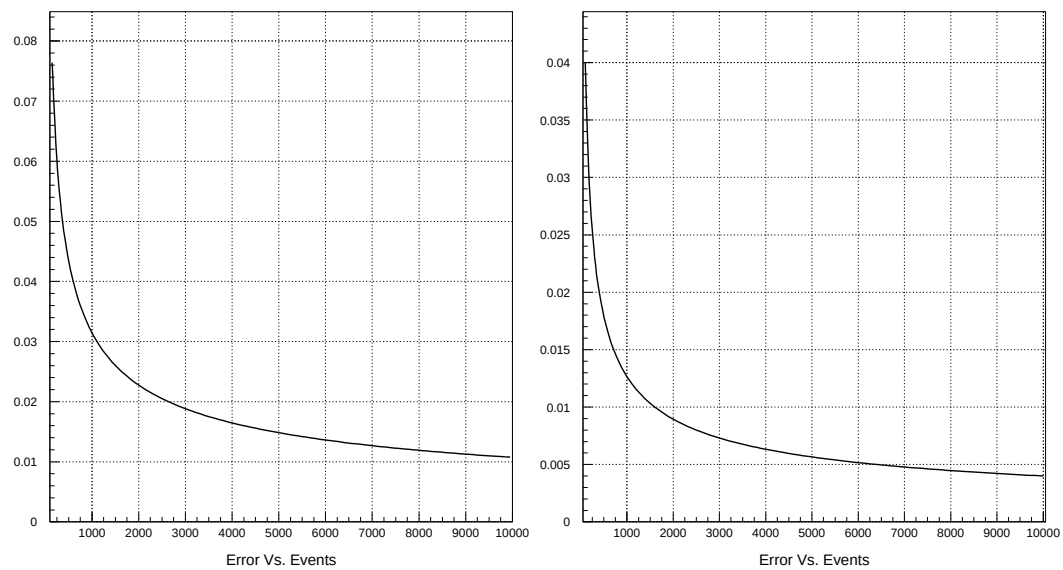

Figure 3.9: Left: The statistical error in $B(t \to bW_{long})$ as a function of sample size. Right: The statistical error in $B(t \to bW_{right})$ as a function of sample size.

Effect	1 fb^{-1}	10 fb^{-1}	100 fb^{-1}
$\delta B(t \to bW_{long})\%$	6.5	2.1	0.7
$\delta B(t \to bW_{right})\%$	2.6	0.8	0.3

Table 3.12: Total precision on top branching fractions to W helicity states

shown in Fig. 3.9. As expected, the statistical error falls as $1/\sqrt{N}$. We see that for sample sizes expected to be available at a high luminosity Tevatron, of order 10K and above, the top quark decay branching fraction to longitudinal W bosons may be measured with a statistical precision approaching 1%, and is systematically limited.

Beyond the benchmark measurement $B(t \to bW_{long})$, full understanding of any non-standard couplings requires a general angular analysis. For instance, the addition of a right-handed decay will not change the branching fraction to longitudinal W, it will only decrease the branching fraction to left-handed W's. We consider a small V+A contribution as a model for potential sensitivity to nonstandard contributions. The right handed W decay distribution is proportional to $(1 + \cos\theta_e^*)^2$ and top decays with a right handed helicity will most likely have $\cos\theta_e^*$ near one. The Standard Model predicts there should be nothing at this $\cos\theta_e^*$, and this analysis is therefore fairly sensitive to right handed decays. To quantify, we add a right-handed term and fit to Monte Carlo experiments of various sizes. The resulting statistical errors are plotted in Fig. 3.9, and indicate that with a sample of order 10K top events a right handed top decay that occurred 5% of the time would appear as a 5σ effect.

The most important sources of systematic uncertainty in these measurements are jet energy and $\not\!\!E_T$ resolution, combinatoric confusion in top decay product assignment, and backgrounds. The resolutions should be well controlled by use of the constrained mass fit algorithm in reconstruction of the final state kinematics. As in the case of the top mass analysis, the contributions of incorrect combinations and backgrounds to the $\cos\theta_e^*$ distribution can be modelled with Monte Carlo and subtracted. Systematic uncertainties from these effects may therefore be considered as equivalent to a reduction of a factor of approximately 2 in statistics and therefore a degradation of order $\sqrt{2}$ in the overall predicted precision. The expected precision, including systematic errors, are shown for the standard sample sizes in Table 3.12.

In conclusion, we have studied the way in which angular correlations in the top final state probe the Wtb vertex. We find that for sample sizes of 10 fb^{-1} the Standard Model prediction for $B(t \to bW_{long})$ and the presence of a V+A term may be probed with precision of a few percent, and that with such a sample these measurements are already systematically limited.

3.5.2 Measurement of a $t \to b$ Branching Fraction and Limit on V_{tb}

In the Standard Model, a 170 GeV/c^2 top quark decays almost exclusively via the $t \to Wb$ mode, because $V_{tb} \simeq 1$, and because there is no kinematic suppression of this decay. The statement $V_{tb} \simeq 1$ *assumes* the unitarity of the CKM matrix, a hypothesis that we would like to test.

Nonstandard model physics can change this value, as well as the interpretation of other phenomena. Suppose there were a fourth generation $(t', b', \sigma, \nu_\sigma)$. This would remove the 3-generation unitarity constraint on V_{tb}, allowing it to be smaller, and thus reduce the $t \to Wb$ branching fraction in favor of $t \to Ws$ or $t \to Wd$. This new generation also influences mixing: there is an additional contribution to K^0, D^0 and B^0 mixing from a box diagram with an t' or b' quark in the loop. Because of the electroweak radiative corrections to the W mass, the t' and b' quarks must be nearly degenerate in mass, which implies that the large difference in the rate of mixing between the slow $D^0 - \overline{D}^0$ and fast $K^0 - \overline{K}^0$ and $B^0 - \overline{B}^0$ systems is a consequence of the relative magnitude of CKM elements, rather than the large t to b mass ratio as in the Standard Model.

In principle, measuring $|V_{tb}|$ is simple. One looks at top events containing W's, and measures the branching fraction into b's:

$$B_b = B(t \to W(b)) = \frac{t \to Wb}{t \to Wq} = \frac{|V_{tb}|^2}{|V_{td}|^2 + |V_{ts}|^2 + |V_{tb}|^2}$$

The notation above is meant to indicate that a W has been required in the final state, and this is not the decay fraction to W+b, but the fraction of decays with W's which *also* contain b's. Since the standard analysis identifies $t\bar{t}$ events by requiring at least 1 W and 1 b, $B(t \to W(b))$ is measured from the number and distribution of tagged b-jets in top events. There are three basic techniques which can be used to measure this ratio:

• The ratio of double b-tagged to single b-tagged events in the b-tagged lepton plus jets sample: Requiring one b jet to be tagged leaves the second jet unbiased, and from a known tagging efficiency, one can extract the branching ratio from the ratio of tagged to untagged "second jets".

• The number of b tagged jets in the dilepton sample: Since b-tagging is not required to identify tops decaying to dileptons, the whole b-tag multiplicity distribution in these events contains information on $B(t \to W(b))$. Despite the smaller branching fraction to dileptons, the statistical power of the dilepton and l+jets samples are comparable.

• The distribution of double tags: If there are two tagging algorithms (soft leptons and secondary vertex), one can compare the number of times that events tagged by both algorithms have both tags in the same jet vs. the number of times the tags are in different jets. Small values of $B(t \to Wb)/B(t \to Wq)$ result in large values of the same to different jet ratio.

These techniques are not exclusive, and can be combined. CDF has used a maximum likelihood estimator to do this combination in Run 1 data. With 67 pb^{-1}, CDF has a $\pm 30\%$ statistical uncertainty on the branching fraction, but only an $\pm 11\%$ systematic uncertainty.

	Run 1	Run 2	Run 3	
Luminosity (fb^{-1})	0.12	1.0	10	100
Event Tag Probability	54%	85%	85%	85%
Tagged l+jets events	40	580	5800	58000
Double-tagged l+jets events	15	300	3000	30000
Same jet double tags	4	90	900	9000
Other jet double tags	12	240	2400	24000
Dilepton events	12	80	800	8000
Tagged dilepton events	7	65	670	6700

Table 3.13: Counting single and double tags

The systematic uncertainty is dominated by the uncertainty on the tagging efficiency, which is measured in the data using b rich inclusive lepton samples. This uncertainty should fall as $1/\sqrt{N}$. The small non-$t\bar{t}$ backgrounds will be measured to high accuracy by Run 2.

We calculate the expected sensitivity for three hypothetical runs with the usual luminosity assumptions: a Run 1 of 120 pb^{-1}, a Run 2 of 1.0 fb^{-1}, and a Run 3 of 10-100 fb^{-1}. The number of expected top events in the various categories is shown in Table 3.13, and the branching fraction uncertainty is shown in Table 3.14. Combining all three methods, we see that 10 fb^{-1} allows the measurement of the branching fraction $B(t \to W(b))$ with a precision of 1%.

	Run 1	Run 2	Run 3	
Luminosity [fb^{-1}]	0.12	1.0	10	100
Single/Double Tag Ratio	1.6 ± 0.5	$0.94 \pm .07$	0.895 ± 0.022	0.895 ± 0.007
$B(t \to Wb)$ Uncertainty	20%	4%	1.8%	0.56%
Different/Same Jet Tag Ratio	2.4 ± 1.0	$2.3 \pm .4$	2.19 ± 0.08	2.189 ± 0.025
$B(t \to Wb)$ Uncertainty	60%	14%	2.6%	0.81%
Dilepton Tag/No Tag Ratio	1.2 ± 0.2	4.9 ± 1.4	5.1 ± 0.5	5.10 ± 0.15
$B(t \to Wb)$ Uncertainty	20%	4.5%	1.4%	0.45%
Overall $B(t \to Wb)$ Uncertainty	15%	3.3%	1.0%	0.33%
Limits on $\|V_{tb}\|$ (95% CL)	> 0.1	> 0.22	> 0.40	> 0.71

Table 3.14: Expected precision on $B(t \to Wb)$ and $|V_{tb}|$

The branching fraction $B(t \to W(b))$ can be used to compute V_{tb} via the following relation:

$$|V_{tb}|^2 = \frac{B_b}{1 - B_b}\left[|V_{td}|^2 + |V_{ts}|^2\right]$$

The branching fraction limits are converted to $|V_{tb}|$ limits under the assumption that $|V_{td}| = 0.009$ and $|V_{ts}| = 0.039$, the midpoints of the 90% CL ranges in the Particle Data Book. Since these values are determined partially by unitarity, this is an assumption (although the correct one to test the Standard Model), and different assumptions of the values of $|V_{td}|$ and $|V_{ts}|$ will produce different relationships between the $|V_{tb}|$ and $B(t \to W(b))$.

Statistical uncertainties for $|V_{tb}| \approx 1$ are shown in Table 3.14. The 95% CL limits on $|V_{tb}|$ from this measurement are > 0.22 with 1 fb^{-1}, > 0.71 in a 100 pb^{-1} Run 3 with one experiment, and > 0.85 with two. It is ironic that the relation between the branching fraction and V_{tb} turns excellent precision on B_b into only modest limits on V_{tb}. An alternative and complementary measurement of $|V_{tb}|^2$ is available in the rate of electroweak $t\bar{b}$ production, and this is discussed in detail in Section 6.

3.5.3 Measurement of a $t \to W$ Branching Fraction

If all top decays proceed through W emission, the ratio of dilepton to single lepton events is $R_l = 1/6$. If some fraction of top decays are through a non-W state with a different branching rate to leptons, the change in the ratio R_l indirectly measures the departure of $B(t \to W)$ from 1.0. In the case where t decays include a non-W state with no leptonic decays, the branching fraction to W's is given in terms of the ratio R_l as

$$B(t \to b(W)) = \frac{9R_l}{1 + 3R_l}$$

The notation above mirrors that used in Sec. 5.2, and indicates that this is the fraction of decays with b's which *also* contain W's. This analysis is obviously model dependent, but consistent with the popular non-standard model that $t \to Wb$ may be augmented with $t \to H^+b$ where in this case $B(H^+ \to c\bar{s}) = 100\%$. Different models for non-standard top decays will obviously require different treatments; the discussion here is meant to be illustrative, and to provide a benchmark for the measurement precision.

The uncertainty on R_l *vs.* luminosity has been estimated in Section 4.2. Propagating this through the above, we find the precision of $B(t \to b(W))$ *vs.* luminosity as given in Table 3.15. With 10 fb^{-1} the ratio of dilepton to single lepton rates in top events will allow determination of the top branching fraction to W's in association with b to a precision of 3.5%. The conversion of this information to a limit on the amount of non-W decay is discussed in the next section.

Effect	1 fb^{-1}	10 fb^{-1}	100 fb^{-1}
$\delta B(t \to b(W))$	10%	3.5%	1.0%

Table 3.15: Statistical error on top branching fractions to W

Luminosity	95% CL limit on $B(t \to Hb)$
1 fb^{-1}	15%
10 fb^{-1}	6%
100 fb^{-1}	1.7%

Table 3.16: Limits on charged Higgs decay

3.5.4 $t \to H^{\pm}b$

A charged Higgs occurs naturally in SUSY models, and for a light charged Higgs, the process $t \to H^+b$ is of interest. The CLEO $b \to s\gamma$ branching fraction [43] appears to place a limit on the Higgs mass ($m_{H^+} > 260$ GeV/c^2), but this limit assumes that there is no destructive interference from a chargino contribution. The decay $t \to H^+b$ could still occur (and in fact, dominate) for large values of $\tan\beta$.

The best direct search strategies are to look for a τ excess from $H^+ \to \tau\nu$ or to find a dijet mass bump from the mode $H^+ \to c\bar{s}$, where the favored mode depends on $\tan\beta$. A study of prospects in the τ mode is underway [45].

There is, in addition, an indirect search technique for this or any other top decay to non-W states. As discussed in Sections 4 and 5.3 (above), the ratio of the top cross section as measured in the dilepton and lepton plus jets channels is sensitive to a missing W component, which manifests itself as a deficit of leptons. Recasting the discussion in 5.3 to measure the *non-W* fraction, we find

$$\frac{\sigma(t\bar{t})_{L+J}}{\sigma(t\bar{t})_{DIL}} \approx 1 + \frac{3}{2}B(t \to H^+b)$$

where the numerator is the $t\bar{t}$ cross section as measured in the lepton plus jets channel and the denominator is the $t\bar{t}$ cross section as measured in the dilepton channel, assuming SM decays. This assumes a 100% branching fraction of the Higgs to $c\bar{s}$, and also assumes an 80 GeV/c^2 Higgs, so that the dijet masses give no separation between $t \to H^+b$ and $t \to W^+b$. In this somewhat pessimistic case, we expect to be able to set limits on this decay to the accuracy given in Table 3.16. For the even more pessimistic case of decays dominated by $H^+ \to \tau\nu$, the limits are approximately a factor of 2 worse.

For a Higgs mass substantially different from the W mass, there is the additional handle of the dijet mass distribution in top events: the Higgs will produce a peak in this distribution, in addition to changing the ratio of cross sections. This will improve the branching fraction limits by an amount dependent on m_{H^+}.

The limits attainable by 10-20 fb^{-1} of $p\bar{p}$ data, in conjunction with the CLEO $B(b \to s\gamma)$ measurement will be enough to exclude (or discover!) $m_{H^+} \leq m_t$ for *any* value of $\tan\beta$.

3.5.5 Rare Top Decays to W, Z, and γ

The presence or absence of certain particle decays can herald the arrival of new physics. For example, the absence of the flavor changing neutral current decay $K_L^0 \to \mu^+\mu^-$ was early evidence for charm, even though the charm quark's mass is three times the mass of the kaon. More recently, observation of the decay $b \to s\gamma$ by CLEO[43] can be used to exclude charged Higgs particles with masses less than 260 GeV/c^2 in some models; a 5 GeV/c^2 particle's decays can be used to probe physics at a mass scale 50 times larger.

As an illustrative example of the reach of rare top decays, we consider the flavor changing neutral current decay $t \to c\gamma$. Standard Model predictions for the branching fractions of FCNC decays are around 10^{-10} [44], so any observation will signal new physics, possibly at very high mass. Here we make estimates of the sensitivity of an upgraded Tevatron collider program to this sort of physics.

There are two signatures for this decay, depending on the decay of the W for the second top in the event. If it decays leptonically, the signature is a lepton, missing E_T, a high E_T photon (usually above 50 GeV), and two jets, one of which is b-taggable. If the W instead decays hadronically, the signature is a high E_T photon, no missing energy, four jets, one of which is b-taggable.

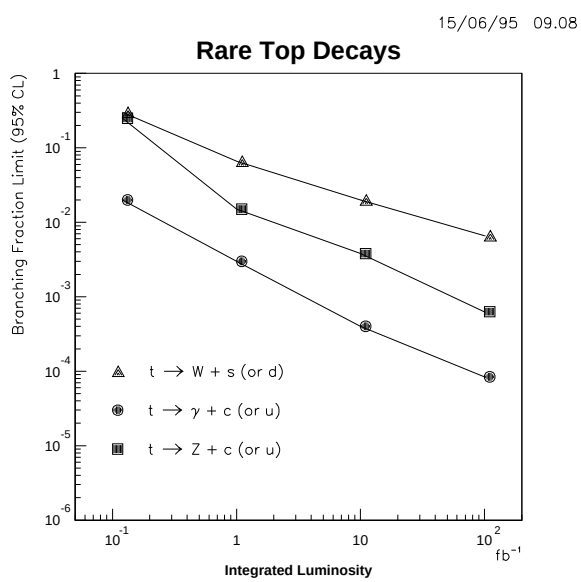

Figure 3.10: Limits on rare top decays

As it turns out, the acceptance of the $c + \gamma$ decay with the second top in the leptonic channel is almost the same as the standard model lepton plus jets mode. The background from $W + \gamma$ (plus two jets) is about 1 fb. Although it is unlikely that this background will be kinematically consistent with $t\bar{t}$ (for example, that $m_{\gamma+j} = m_t$), we take the very conservative assumption that this background is irreducible. It is then straightforward to scale from the number of observed events in the lepton plus jets mode to the 95% limit on

this branching fraction.

A 120 pb^{-1} Run 1 will yield about 40 tagged tops at CDF, and with a tagging efficiency of about 55% per event, this corresponds to a limit of approximately 4%. By a 1 fb^{-1} Run 2, assuming one background event is seen, the limit from each experiment would be approximately 5.7×10^{-3}.

Things are somewhat different by a 10 (or 100) fb^{-1} Run 3. At this point there will be 10 (100) background events; to set a limit, we would need to apply an additional selection, such as b-tagging. This will reduce the efficiency (and thus the limit) by about 60% (there is only one b to tag) but with 6K (60K) top events, a limit of 6.2×10^{-4} (1.3×10^{-4}) per experiment can be achieved, assuming zero (two) background events survive the b tagging. We emphasize that this is entirely without kinematic requirements.

The case where the second top decays hadronically is somewhat harder to estimate. There are certainly many high p_T photons with 4 jets from QCD processes, and a small fraction of them have real $b\bar{b}$ in them. It appears that both b tagging and kinematic cuts will have to be applied. We assume that the kinematic cuts will be 100% efficient in Run 1, 50% efficient in Run 2, and 30% efficient in Run 3, although it must be stressed that these are estimates: we haven't integrated enough luminosity to date to measure the background to this decay reliably. The expected limits, assuming one remaining background event in Runs 2, zero in a 10 fb^{-1} Run 3, and two by a 100 fb^{-1} Run 3, are shown in Table 3.17.

	Run 1	Run 2	Run 3	
Luminosity	120 pb^{-1}	1 fb^{-1}	10 fb^{-1}	100 fb^{-1}
$l + \gamma$+2 jets limit	4%	5.7×10^{-3}	6.2×10^{-4}	1.3×10^{-4}
γ+4 jets limit	4%	6.5×10^{-3}	1.1×10^{-3}	2.4×10^{-4}
Overall limit	2%	3.0×10^{-3}	4.0×10^{-4}	8.4×10^{-5}

Table 3.17: Sensitivity for $t \to c\gamma$.

	Run 1	Run 2	Run 3	
Luminosity	120 pb^{-1}	1 fb^{-1}	10 fb^{-1}	100 fb^{-1}
$3l$+2 jets limit	50%	4.3%	7.4×10^{-3}	1.0×10^{-3}
$2l$+4 jets limit	50%	2.6%	7.9×10^{-3}	1.7×10^{-3}
Overall limit	25%	1.5%	3.8×10^{-3}	6.3×10^{-4}

Table 3.18: Sensitivity for $t \to Zc$.

Note that the two search modes are roughly comparable. (It is also of interest that the CLEO $b \to s\gamma$ branching fraction is $(1.87 \pm 0.67) \times 10^{-4}$ [43]. With two comparable experiments at the Tevatron, the equivalent level of sensitivity for $t \to c\gamma$ is reached at about 11 fb^{-1}.)

Sensitivity to other rare decays can be scaled from this estimate. For example, one can consider $t \to Zc$, where the Z decays to leptons. The acceptances are similar, but one needs to consider the Z branching fraction to leptons of 6.7%, compared to the photon reconstruction efficiency of about 80%. To first order, the limits will be a factor of 12 worse. However, the trilepton backgrounds are substantially smaller than the $W\gamma$ backgrounds: about a quarter of an event in Run 2 (without a b-tag) and a third of an event in a 100 fb^{-1} Run 3 (with a b-tag). Here we assume zero observed background events until 100 fb^{-1}, where we assume one. For the hadronic decays of the W, the backgrounds are again lower. We are assuming that only b-tagging is necessary in Runs 1 and 2 (where 0.06 and 0.5 background events are expected) and kinematic cuts that are 50% efficient (with a remaining background of .02 events/fb^{-1}) are necessary in Run 3. Expectations for this search are summarized in Table 3.18 and Fig. 3.10.

There are other rare decays, such as $t \to WZb$. This mode is interesting because it is close to threshold and might provide an accurate measure of the top mass and also because it directly probes the $t - t - Z$ vertex. As long as the backgrounds are small, as they often are for these rare modes, the sensitivity scales as $1/N$, rather than $1/\sqrt{N}$. Modest increases in running time, luminosity, acceptance and efficiency can contribute to substantial improvements in physics reach.

Although this section has been written in terms of limit estimates, we wish to emphasize that there is a more exciting prospect ahead of us, *discovery* of these rare decays, which would cause us to rethink our understanding of high mass physics.

3.6 The Physics of Single Top Quark Production

The preceding discussion has focussed on physics capabilities with the dominant top production mode, strong production of $t\bar{t}$ pairs. However, top quarks can also be produced singly via the electroweak interaction [46, 47, 48], and this process offers an interesting and complementary program of measurements. The principal processes leading to single top production are shown in Fig. 3.11, along with their higher order corrections. The first process $q'\bar{q} \to t\bar{b}$, proceeds via an s-channel W^* and the second, $qb \to q't$, involves a t-channel W. We will refer to the first process and its corrections as "W^*", and the second process, together with its corrections ($qg \to q't\bar{b}$), as "W-gluon fusion". Other processes, such as $gb \to tW$, are important at higher energies, but contribute only a few percent to the rate at 2.0 TeV.

The cross sections for all top production mechanisms in $p\bar{p}$ collisions at $\sqrt{s}$=2.0 TeV are shown in Fig. 3.12 [9, 49]. For $m_t = 170$ GeV/c^2, W-gluon fusion, at 1.6 pb, is twice as large as W^* at 0.8 pb, and the combined rate for single top production by these two processes, ~ 2.4 pb, is over a third of the $t\bar{t}$ rate at this energy. Single top studies at the Tevatron will have good statistical power.

The production of a $t\bar{b}$ pair from a W is closely related to the decay of a t quark through a Wb, and the the single top cross section turns out to be directly proportional to the partial width $\Gamma(t \to Wb)$. As shown at the beginning of Section 5, $\Gamma(t \to Wb)$ is a function of both the decay couplings and $|V_{tb}|^2$. The single top sample will provide a very accurate measurement of the decay width, and in the absence of anomalous couplings this is

Figure 3.11: Representative Feynman diagrams for single top quark production at the Tevatron: (a) W^* boson s-channel $p\bar{p} \to t\bar{b}$ + X; (b) W boson t-channel $p\bar{p} \to tq$ + X; (c) $p\bar{p} \to tW$ + X.

an accurate measure of $|V_{tb}|$. This sample is also an independent top laboratory with some unique physics opportunities described later.

We present here a study of single top quark yields using Monte Carlo parton level events combined with simple parametrizations of detector effects. We then estimate the potential accuracy of a number of possible measurements as a function of the data sample size.

3.6.1 Single Top Quark Simulation

Simulations of electroweak single top production and the principal backgrounds have been performed using the ONETOP Monte Carlo [42, 48]. Two different values of the mass of the top quark are used, 170 and 200 GeV/c^2, and the center of mass energy of the $p\bar{p}$ collisions is set to 2.0 TeV.

The ONETOP program makes a tree level calculation of the two main signal processes. The $qb \to q't$ cross section was scaled to the total tree level W-gluon fusion cross section, which properly accounts for the higher order process $qg \to q't\bar{b}$ [50], and this rate was then added to the $q\bar{q}' \to t\bar{b}$ cross section. We use the ONETOP default scale factors and parton distribution functions. $Q^2 = M_Z^2$ for all processes except $t\bar{t}$ where the average value of the transverse mass is taken as the scale. The CTEQ2L leading order fit [51] is used for the parton distribution function.

The ONETOP simulation decays the top quark into bW^+ with $W^+ \to e^+\nu_e$. In calcu-

Figure 3.12: Electroweak single top production cross section from $p\bar{p}$ interactions (LO), with the top quark pair cross section (resummed NLO) shown for comparison.

lating our yields for these processes we double the number obtained from the Monte Carlo once to account for $W^+ \to \mu^+\nu_\mu$, and again to account for the $\bar{t}$ antiquark charge conjugate processes. In the background processes, ONETOP also decays the W^+ into $e^+\nu_e$ and the muonic decays are again accounted for by simply doubling the yields.

In our simulations and yield calculations we take the b-tagging efficiency (per jet) to be 50% [52]. This figure includes geometrical acceptance within the fiducial volume of the detector, and intrinsic silicon microstrip detector efficiency, as well as the efficiency for the secondary vertex finding algorithms. The probability of incorrectly tagging a gluon or light quark jet as a b jet, known as the mistag probability, is taken as 0.4%, based on the current CDF silicon vertex detector experience. The lepton identification efficiency is taken to be 70% [53], which includes factors for the efficiencies of the triggers as well as the reconstruction.

Parton and lepton momenta are smeared according to the resolution functions of the current DØ detector [54]. The charged lepton energy resolution is parametrized using $15\%/\sqrt{E} \oplus 3\%$. The final state quarks are treated as jets and so their energy is smeared using $82\%/\sqrt{E} \oplus 18\%$. The missing transverse energy is recalculated after smearing the jet energies. Note that the constant term in the energy resolution will be greatly reduced in Run 2, and that the mass resolution may be considerably better than what we find below.

3.6.2 Single Top Analysis

We perform an example analysis using the following data selection criteria:

- Exactly two jets with $E_T > 20$ GeV, $|\eta|_{\text{jets}} < 2.5$

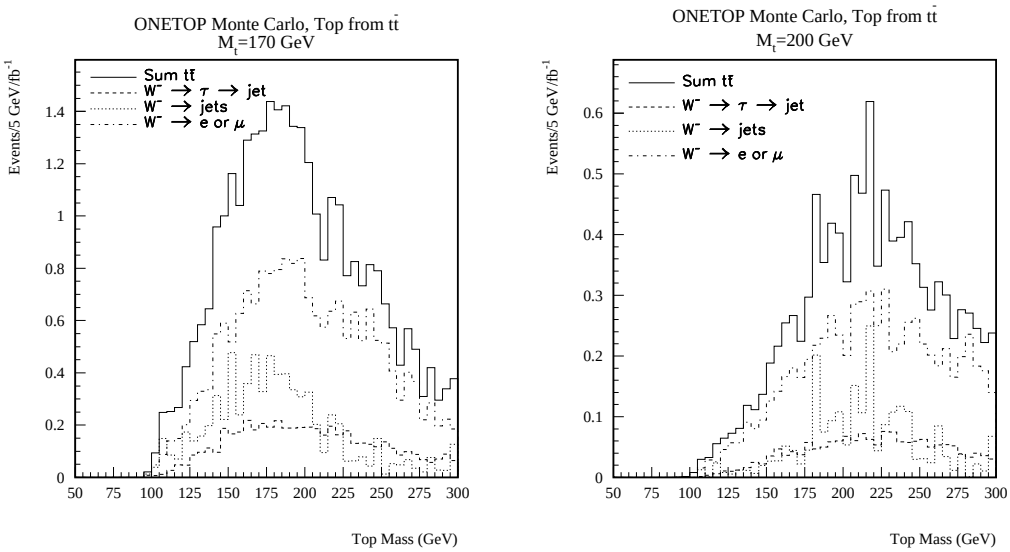

Figure 3.13: Wb mass distribution for $t\bar{t}$ background processes in single top analysis, with (a) a 170 GeV/c^2top quark and (b) a 200 GeV/c^2top quark.

- $\Delta R = \sqrt{(\Delta\phi)^2 + (\Delta\eta)^2} > 0.5$ between all jet pairs and jet-electron pairs
- $E_T(\text{electron}) > 20$ GeV
- $|\eta|_{\text{electron}} < 2.5$
- Missing $E_T > 20$ GeV
- No second isolated electron present with $E_T > 20$ GeV
- At least one jet tagged as a b jet.

The signal for single top production is a peak in the Wb invariant mass plot. The x and y components of the neutrino momentum are taken from the vector missing E_T. The z component is then calculated by requiring that the invariant mass of the electron and neutrino equal the W mass. There are generally two solutions which satisfy this constraint. The solution with the smaller $|p_z|$ is selected.

In the real data one does not know *a priori* which jet is the b jet arising from the top quark decay. Even with detached vertex b-tagging, some of our signal processes have a $\bar{b}$ jet produced together with the top quark, giving some ambiguity. In our analysis, if both b jets are tagged, the jet with the largest (most positive) η is selected. The charge of the W distinguishes between top quark and $\bar{t}$ antiquark candidates. For antitop one would choose the more backward jet (most negative η). We have compared the signal shape obtained with this technique to the shape obtained using the known b jet from the Monte Carlo. The shapes are quite similar, with a small broadening in the channels where confusion with the $\bar{b}$ quark is possible.

The principal background sources for single top production are $q'\bar{q} \to Wb\bar{b}$ and $q\bar{q}, gg \to t\bar{t}$. Most other backgrounds, such as WW and WZ, will be very small after suitable cuts. Imperfect b jet identification will lead to other backgrounds, as discussed below.

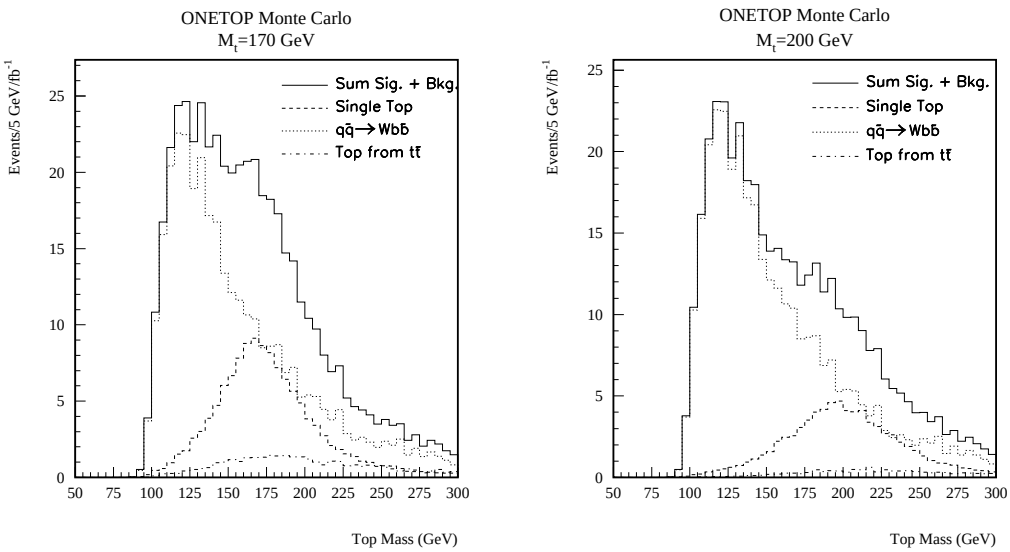

Figure 3.14: Wb mass distribution for single top signal and background processes, with (a) a 170 GeV/c^2top quark and (b) a 200 GeV/c^2top quark.

The $Wb\bar{b}$ background has been scaled to agree with current CDF $t\bar{t}$ analysis [11]. The ONETOP Monte Carlo was run at $\sqrt{s} = 1.8$ TeV with current CDF $t\bar{t}$ selection cuts, and the program's $Wb\bar{b}$ yield was compared to the CDF b-tagged yield of $Wb\bar{b}, Wc\bar{c}$ and Wc events (with mistags excluded). The Monte Carlo was found to overestimate the actual yield, and a correction factor of 0.6 has therefore been employed. The "$Wb\bar{b}$" yields in Table 3.19 therefore also account for backgrounds from $Wc\bar{c}$ and Wc events. (The lifetime of the c quark and the larger $Wc\bar{c}$ cross section cause about a third of the single tagged "$Wb\bar{b}$" sample to actually come from c quarks.)

Light quark and gluon jets can also contribute to the background. The mistag rate with the current CDF silicon vertex detector is 0.5% per jet and a smaller mistag rate is expected for Run II detectors. If we take this rate to be 0.4%, then because the $Wb\bar{b}$ cross section is roughly 0.01 of the total Wjj cross section, the background from Wjj will be the same size as the background from $Wb\bar{b}$ with 50% b-tagging efficiency. We therefore account for the Wjj background by simply doubling the size of the $Wb\bar{b}$ background. We also assume here that the shape in the mass plot for Wjj events is the same as that for $Wb\bar{b}$; studies show this to be a reasonable assumption. The "Wjj" line in Table 3.19 reflects this doubling, and the "$Wb\bar{b}$" mass distribution in Fig. 3.14 is just the calculated $Wb\bar{b}$ distribution doubled to include the effect of Wjj. All three backgrounds ($Wb\bar{b}$, Wjj and $t\bar{t}$) are included when calculating the uncertainties in Table 3.20.

We note here that one can reduce the $Wb\bar{b}$ background by about a factor of two by increasing the cut on E_T(jet 1) from 20 to 40 GeV. This is not entirely advantageous, however, because this causes the background to peak in the signal region. The optimal value of this cut for single top signal extraction will depend strongly on the top quark mass.

No scaling was applied to the $t\bar{t}$ background as the Monte Carlo cross sections from ONETOP (7.2 pb at $m_t = 170$ GeV/c^2, 3.0 pb at $m_t = 200$ GeV/c^2, $\sqrt{s} = 2.0$ TeV) agree with expectations from the measured values at $\sqrt{s} = 1.8$ TeV. In Figs. 3.13(a) and (b), the composition of the $t\bar{t}$ background is shown in more detail. In our Monte Carlo the W^+ from top always decays to a positron and a neutrino (and we double the yields to include the

	m_t = 170 GeV/c^2		m_t = 200 GeV/c^2	
	Yield/fb^{-1}	Peak Region/fb^{-1}	Yield/fb^{-1}	Peak Region/fb^{-1}
single top signal	123	107	76	63
Wbb background	163	109	163	63
Wjj background	163	109	163	63
$t\bar{t}$ background	32	21	11	7

Table 3.19: Yields for single top analysis. The "peak region" is within 50 GeV/c^2 of the generated top quark mass. The jets in the Wjj background are gluons and light quarks where one jet is mistagged as a b quark.

contribution from W^+ to muon and neutrino). The W^- from $\bar{t}$ decay is then treated for the three separate cases of decay to electron or muon, decay to tau (followed by tau decay to hadrons), and decay to jets. With these cuts, the jets contribution is negligible (due to the requirement of only two jets in the final state) and the $t\bar{t}$ background comes primarily from the dilepton channel (where the second lepton is either not isolated, is outside the fiducial region, or has a $E_T < 20$ GeV).

We have considered the background contribution from QCD multijet events, where one jet is misidentified as a lepton and there is a mismeasurement of the jet energies leading to large missing E_T which fakes a neutrino. In the current CDF W+jets event sample, it is estimated that ~10% is actually QCD multijet events, which means the misidentified QCD multijet events will add an additional 11% (one fake W for every nine real W's) to the $Wb\bar{b}$ and Wjj backgrounds included in the calculation.

The single top signal is presented in Fig. 3.14 and Table 3.19, together with the contributions from the $Wb\bar{b}$, Wjj, and $t\bar{t}$ backgrounds, for two different top masses. The vertical scales in Fig. 3.14 have been normalized to give the expected numbers of events in 1 fb^{-1} of Run II data. In each plot the summed signal and background curve is easily distinguished from the background shape alone. The cross section is lower for the 200 GeV/c^2 top quark, but the peak is out in a region of smaller background, so the signal to noise is similar to the case of the 170 GeV/c^2 top mass. At the time of Run II, the top mass should be well enough known and the signal shape well enough understood that the peak will be easily picked out above a smooth background in fits to the data. Event yields can then be extracted from the area of the signal shape in these fits.

3.6.3 The Single Top Quark Cross Section

The single top cross section may be obtained from the mass plots in a straightforward manner. We calculate the fractional statistical uncertainty in the cross section as $\sqrt{S+B}/S$, where the size of signal (S) and background (B) are the numbers of each kind of event in the mass peak window of 50 GeV/c^2 around the generated top quark mass. The results are summarized in Table 3.20 for our two input top masses of 170 and 200 GeV/c^2. For the case m_t = 170 GeV/c^2 we find that 10 fb^{-1} will allow measurement of the single top cross

	$m_{top} = 170\text{GeV}/c^2$	$m_{top} = 200\text{GeV}/c^2$
S/B	0.45	0.47
% error with 2 fb^{-1}	12.3	15.7
% error with 10 fb^{-1}	5.5	7.0
% error with 100 fb^{-1}	1.7	2.2

Table 3.20: Signal to background ratio and estimated statistical error for 2, 10, and 100 fb^{-1}.

Effect	1 fb^{-1}	10 fb^{-1}	100 fb^{-1}
$\delta\sigma_{t\bar{b}X+b\bar{t}X}$	26%	10%	7%
$\delta\Gamma(t \to Wb)$	28%	12%	10%
$\delta\|V_{tb}\|$	14%	6%	5%

Table 3.21: Measurement precisions in the single top program.

section with a statistical precision of 5.5%.

Many of the sources of systematic uncertainty in the single top cross section are common to the $t\bar{t}$ cross section measurement discussed in Section 4. We assume that systematic uncertainties related to selection efficiencies and backgrounds will shrink as $1/\sqrt{N}$ and find that for large samples the dominant uncertainty is that of the luminosity normalization. The cross section precisions for our standard luminosity benchmarks are shown in Table 3.21 for $m_t = 170$ GeV/c^2. For the case of 10 fb^{-1} we find that the measurement of the single top cross section will have a total uncertainty of approximately 10% [56].

3.6.4 Top Quark Decay Width and $|V_{tb}|$ from Single Top

At a hadron collider, the top quark decay width $\Gamma(t \to X)$ cannot be directly measured in the $t\bar{t}$ sample, but its main component can be accessed through single top processes. The single top cross section is directly proportional to the partial width $\Gamma(t \to Wb)$ and, assuming there are no anomalous couplings, this is a direct measure of $|V_{tb}|^2$.

We have made a detailed study of the extraction of $\Gamma(t \to Wb)$, and $|V_{tb}|^2$ from the combined single top cross section [55, 56]. The constant of proportionality between the cross section and the width has theoretical uncertainties originating in α_s, the parton distribution functions, and the choice of scale Q^2. These are estimated to total roughly 10% at present [57], and we assume that better measurements of parton distributions and $\sigma_{t\bar{t}}$ will improve this to 7%. Combining all uncertainties yields anticipated precisions on $\Gamma(t \to Wb)$ and $|V_{tb}|^2$ as displayed in Table 3.21. We find that a measurement of the inclusive single top cross section with 10 fb^{-1} will yield the partial width $\Gamma(t \to Wb)$ with precision of 12%, and therefore V_{tb} with a precision of 6%.

3.6.5 Isolation of the W^* Process and a Separate Measurement of $|V_{tb}|$

If large data sets are available, it may be that the width is best found by measuring the single top rate from the W^* s-channel process separately from the W-gluon fusion process. The theoretical determination of the $q'\bar{q} \to W^* \to t\bar{b}$ rate is less prone to the uncertainties involved in the W-gluon fusion calculation since initial state effects can be measured in the similar Drell-Yan process $q'\bar{q} \to l\nu$. Reference [58] discusses prospects for isolating the W^* piece of the single top signal at the next Tevatron run. Their strategy is to require that both jets be tagged as b jets. In addition, they require no more than two final state jets, which substantially reduces the W-gluon fusion background, leaving only some small fraction of $qg \to q't\bar{b}$, where the light quark jet has escaped detection.

We now modify our earlier analysis to require that both jets be tagged as b jets. We also adopt two additional cuts from Ref. [58]: $\Delta R_{b\bar{b}} > 0.7$ and $M_{b\bar{b}} > 110$ GeV/c^2. These cuts serve to provide needed additional reduction of the $Wb\bar{b}$ background. For $m_{top} = 170$ GeV/c^2, we obtain yields per fb^{-1} in the peak region (as defined in Table 3.19) of 8.1 events from the W^* process, 2.1 events from W-gluon fusion, 6.7 events from $Wb\bar{b}$, and 3.0 events from $t\bar{t}$. This gives a total number of background events per fb^{-1} of $B = 11.8$ compared to a signal of $S = 8.1$. We ignore the Wjj background here due to the double b jet tag. The fractional statistical error, $\sqrt{S+B}/S$, would thus be 39% with 2 fb^{-1} of data, 17% with 10 fb^{-1}, and 5.5% with 100 fb^{-1}.

The authors of Ref. [58] use a different Monte Carlo program, make different cuts and different detector assumptions, use a slightly different top quark mass (175 GeV/c^2), and include additional backgrounds, but their conclusions are similar. They find that, assuming $|V_{tb}|$ is close to unity, 12 fb^{-1} of integrated luminosity yields a 10% measurement of the partial width $\Gamma(t \to Wb)$ and hence a 5% measurement of $|V_{tb}|$. Our more pessimistic detector parameters account for much of the difference between the analyses. In either case, the balance between systematics and statistics in the W^* measurement yields a final precision on $|V_{tb}|$ which is comparable to the result of using the full single top sample. It will be interesting to see how these differences play out in the real measurement.

Ref. [58] also suggests that the W^* signal could be difficult to extract at the LHC. The $t\bar{t}$ and W-gluon fusion backgrounds are relatively larger than at the Tevatron because they are initiated by gluons, while the signal is a quark-antiquark annihilation process and is thus heavily suppressed. At the LHC these backgrounds are each about twice as large as the signal, and have the same shape in the invariant mass m_{Wb} spectrum.

3.6.6 Other Physics Measurements with Single Top

In Standard Model single top production, the top quark is produced from a left-handed W boson resulting in a significant polarization of the top spin in the direction of the b in the $W*$ process and in the direction of the light quark in the W-gluon fusion process [59]. Since the top spin information is preserved in the final state (because the top decays before it can hadronize) this polarization may provide additional handles on the single top signal. In addition, if there are non-standard sources of CP violation in top decay, this polarization

will make their detection much simpler.

One can also look for CP violation in the production of the top quark. Since the initial $p\bar{p}$ state is a CP eigenstate, any difference between the cross sections for $p\bar{p} \to tX$ and $p\bar{p} \to \bar{t}X$ is a signal for CP violation. From our calculated event yields, and assuming $\sigma(p\bar{p} \to tX) \approx \sigma(p\bar{p} \to \bar{t}X)$, we can estimate the precision to which we can measure any asymmetry using:

$$A = \frac{\sigma(p\bar{p} \to tX) - \sigma(p\bar{p} \to \bar{t}X)}{\sigma(p\bar{p} \to tX) + \sigma(p\bar{p} \to \bar{t}X)}.$$

Taking the mass peak region yields for the 200 GeV/c^2 top quark, we see that the absolute statistical uncertainty in A is 0.16 with 2 fb^{-1} of data, 0.07 with 10 fb^{-1} and 0.02 with 100 fb^{-1}.

Finally, we note that the top quark mass will be determined from single top events with different systematic errors than those found in the $t\bar{t}$ analysis. The jet-parton combinatorics are less severe, since there are fewer jets and the correct b jet to combine with the W can be identified more often. Our model simulation does not include the detailed effects of gluon radiation, multiple interactions, or the underlying event, so no conclusions can be reached here about the possible accuracy of the mass determination, but we believe it will be an interesting and useful independent measurement.

3.6.7 Conclusions for Single Top

We have demonstrated the capability of isolating the "electroweak" production of single top. The production rate for this process is proportional to the partial top width $\Gamma(t \to Wb)$ which measures the product of $|V_{tb}|^2$ and the top decay couplings. In the absence of anomalous couplings, 10 fb^{-1} at the Tevatron will allow determination of $|V_{tb}|$ to an accuracy of approximately 6%. With larger samples it will be possible to isolate the W^* component of single top production, allowing determination of $|V_{tb}|$ with somewhat larger statistical error than above, but better control of theoretical uncertainties. Finally, since our simulations show that it is reasonably straightforward to extract a signal from data gathered at a high luminosity Tevatron, we are optimistic that other interesting areas of the single top physics program will also be realized.

3.7 Top Physics at Other Facilities

3.7.1 NLC

An extensive literature exists on the potential for top physics at a high energy e^+e^- collider (see [60, 63] and other papers in these collections). We review here a few illustrative issues.

Since the massive top decays before hadronizing, there is no toponium resonance. For $m_t = 175$ GeV/c^2, the cross section rises smoothly from 0.6 pb at threshold to 1.4 pb at $E_{cm} = 500$ GeV. There are backgrounds from W pair production with $\sigma \sim 10$ pb, and $q\bar{q}$ + ISR + gluons with $\sigma \sim 30$ pb. Most studies use kinematic discrimination to isolate the top

signal, and suggest selection efficiencies of $\sim 50\%$ for all decay modes [60]. At threshold, the yield is 600 events per fb^{-1} in all modes. If at least one $W \to l\,\nu$ decay is needed to suppress combinatoric background in final state fits [63], the yield will be ~ 100 events per fb^{-1}.

The yield is low, but control of the initial state offers some interesting possibilities. The structure of the production cross section at threshold is a function of m_t and α_s, and somewhat more weakly of Γ_t and λ_{tH}, the Higgs Yukawa coupling. The analysis of Ref. [64] supposes a scan of 9 points in the threshold region, with 1 fb^{-1} per point, assuming that the center of mass energy can be known with precision better than 10^{-3}. In this case, the expected precisions for $m_t = 180$ GeV/c^2 are $\delta m_t = 500$ MeV/c^2 and $\delta\alpha_s = 0.009$. Ref [61] suggests that if m_t and α_s are known with infinite precision, a second scan with comparable luminosity could yield a 50% measurement of Γ_t and λ_{tH}, although the width measurement is difficult for $m_t \geq 150$ GeV/c^2.

The crux of these measurements is control over E_{cm} in a linear collider. The intrinsic energy spread is typically 0.1-1.0% [65], and this is further degraded by "beamstrahlung" and initial state radiation, but the discussion in Ref. [64] suggests that the resulting "luminosity spectrum" can be reconstructed by monitoring the spent beams and small angle Bhaba scattering. The very precise control of operating conditions, not to mention extended running off the peak energy, suggest that threshold measurements in the top system will occur somewhat later in the full program of measurements at a linear collider.

Besides the top threshold behavior, a number of other measurements are possible in the top sample which can be accumulated at a linear collider. The study of couplings at the production vertex is unique to e^+e^-, and there is a natural top polarization correlated with a forward-backward asymmetry which may have utility in this regard [62]. A simulation study suggests that 50 fb^{-1}would allow the measurement of the static form factors at production and decay with a precision of a few percent [66]. In the case of measurements which depend on the final state only, such as rare decays, we would expect comparable sensitivities between similar sized samples at any facility.

3.7.2 LHC

Top physics at the LHC will be done primarily during the early running at relatively low luminosities of $10^{32} - 10^{33}$cm^{-2}s^{-1}. At the full luminosity of the machine it is expected that multiple interactions will render b-tagging ineffective and thereby make top physics much more difficult. In pp collisions at the final LHC energy of $\sqrt{s}$=14 TeV the $t\bar{t}$ production cross section is about 100 times larger than that at the Tevatron. If the low luminosity running at the LHC turns out to be equivalent to a typical calendar year at 10^{33}cm^{-2}s^{-1}, or 10 fb^{-1}, and detection efficiencies are roughly similar, the LHC experiments will have a statistical advantage of approximately two orders of magnitude over a 10 fb^{-1} Tevatron run. In comparing top measurements at the Tevatron with similar measurements at LHC it is clear that in most cases the statistical advantage will be significant. Below, we briefly review the LHC version of each of the Tevatron measurements discussed in the preceding pages.

A. Mass Measurement

Statistical uncertainties in the top mass measurement with 2 fb^{-1} are already quite

small at the Tevatron, when compared to the systematic uncertainties. At the LHC, the statistical uncertainty will be negligible. As discussed in Section 3, systematic effects on the measurement are studied, in large part, using control samples in the data, and uncertainties due to many systematic effects are therefore likely to scale with $1/\sqrt{N}$. Systematics due to b-tagging bias are already small with 2 fb^{-1} at the Tevatron and should remain negligible at LHC. Another major systematic uncertainty is that due to the shape of the background. As discussed in Section 3, this can be controlled with a sufficiently large sample of Z+4 jet events, which will certainly be accumulated at LHC. The major systematic top mass uncertainty at LHC is likely to be, as it is at the Tevatron, related to the jet energy scale. With a sufficiently large sample of $t\bar{t}$ events, much of the energy scale uncertainty can be calibrated away *in situ* using the $W \to q\bar{q}$ mass peak in $t\bar{t}$ events (see Sec. 3.4B). This will certainly be an effective technique at LHC and the light quark jet energy scale uncertainty should be quite small. Uncertainties in the b jet energy scale can, in principle, be controlled using $Z \to b\bar{b}$ events or possibly $WZ \to \ell\nu b\bar{b}$, if such samples can be isolated. As mentioned in Section 3, there is significant resolution broadening which results from hard gluon radiation, and here the situation at LHC will be worse than that at the Tevatron as a result of the higher energy. We have found no detailed studies of these effects at LHC energies, so it is difficult for us to quantify the effect on the mass resolution, but it is the one feature of the mass measurement in which the Tevatron is at an advantage over LHC. It should be mentioned that the 'extra jet' effect can be somewhat ameliorated by careful event selection, such as requiring four and only four jets, which becomes effective only when there are sufficient statistics.

The ultimate precision of the LHC mass measurement is somewhat difficult to gauge. Many of the systematic uncertainties will scale down statistically from the values cited in Section 3 for the Tevatron. Uncertainties which *do* scale this way are likely to be negligible in the overall scheme of things at LHC. It is therefore those effects which *don't* scale as $1/\sqrt{N}$ that will determine the ultimate sensitivity. It is likely that the gluon radiation effects mentioned above will be in this category, but it is nearly impossible to predict where the "brick wall" will be reached in controlling these effects. The LHC literature [67] quotes an ultimate mass uncertainty of $\pm$ 2 GeV/c^2. Given the recent Tevatron experience, this seems quite conservative and it is likely that the final result will be better than this, perhaps as small as $\pm$ 1 GeV/c^2.

It is perhaps worth noting that the obvious application of an accurate top mass is in the precision electroweak program, and, even assuming the best measurements possible by the year 2005, this program is limited by other factors (δm_W, $\alpha_{em}(Z)$, etc) for top mass precision better than 2 GeV/c^2. See Chapter 4, Section 2.4, for further details.

B. Production Cross Section

This is a measurement which at LHC is quite complementary to the measurement at the Tevatron. The ultimate uncertainty at the LHC is likely to be limited, as it is at the Tevatron, by the knowledge of the integrated luminosity. As a test of QCD, one clearly wants both the Tevatron and LHC measurements. In terms of searching for non-Standard Model production mechanisms such as resonance production, the LHC presumably has more reach as a result of the higher energy. However, this conclusion depends somewhat on exactly what the presumed resonance is. Since $t\bar{t}$ production at the LHC is primarily via gluon fusion, it

is insensitive to a spin-one color singlet, whereas at the Tevatron where $t\bar{t}$ production is a $q\bar{q}$ process, there is no such restriction.

C. Wtb Couplings

The statistical uncertainties in the measurement of the fraction of longitudinal and right-handed W bosons at LHC drop by a factor of 10-30 compared to the Tevatron numbers quoted in Table 12 of Section 5.1. Therefore the LHC measurement uncertainty is likely to be dominated by systematic effects. These systematic effects are the same as those mentioned in 5.1 and are similar to the systematic effects seen in the mass measurement. As with the LHC mass analysis discussed above, it is difficult to quantify where the uncertainties will plateau, but a factor of at least 2-3 improvement over the Tevatron uncertainties seems a reasonably conservative expectation.

D. Rare Decays

The Standard Model rates for FCNC are unobservable even at the LHC. With a factor of 100 improvement in statistics, the LHC clearly has more reach for detection of non-Standard Model branching fractions. For $t \to Ws$ the Standard Model prediction is of order 10^{-3}. In principle this might be observable at the LHC, but without detailed studies of efficiencies and backgrounds it is far from certain.

E. Single Top Production

Single top production via the W-gluon fusion process discussed in Section 6 can be detected at LHC with comparable or slightly better S/B as at the Tevatron. The extraction of $|V_{tb}|$ from the measured cross section will suffer from the same uncertainty from the gluon distribution as at the Tevatron.

For single top produced by the s-channel W^* process, however, one expects approximately a 6% uncertainty on the measurement of V_{tb} (see Section 6.4), and this measurement is likely to be better at the Tevatron than at LHC. The reason is that at the Tevatron one can effectively separate the W^* from the W-gluon fusion events by vetoing on the presence of an additional jet [58]. The growth in cross section for single top production via W-gluon fusion and $t\bar{t}$ production (via glue-glue) between $\sqrt{s} = 2$ TeV and $\sqrt{s} = 14$ TeV is much greater than that for single top production via W^*, which is a valence $q\bar{q}$ process. As a result, the W^* signal is swamped by W-gluon fusion and $t\bar{t}$ events at LHC, even after the additional cuts are applied.

3.8 Conclusions

We have reviewed the prospects for a top physics program at the Fermilab Tevatron in the Main Injector Era. The conclusions are preliminary, but have the strength of being extrapolations from real measurements in the well understood environments of the present day Collider experiments.

The results are summarized in Table 3.22. The CDF and DØ experiments will each record over 500 identified $t\bar{t}$ events per fb^{-1}. With an integrated luminosity in excess of 10 fb^{-1}: the top mass will be measured with an accuracy of 2 GeV/c^2; the total cross section measurement will be limited only by the luminosity normalization precision, presently 5%, and non-standard production mechanisms will be resolvable down to total cross sections of $\sim$ 25 fb; the branching fraction to b quarks and branching ratio to the various W helicity states will be measured with with precisions of order 1-2%; the branching fraction to non-W states may be explored at the level of 5%; and the magnitude of a FCNC decay will be probed down to branching fractions of 0.1%. We have demonstrated the capability to isolate the electroweak production of single top, where the production rate is proportional to the partial width $\Gamma(t \to Wb)$. A data set in excess of 10 fb^{-1}will allow determination of $\Gamma(t \to Wb)$ to 12%, and inference of $|V_{tb}|$ with a precision of 6%.

We believe that this is only the beginning of the catalog of top physics measurements at the Tevatron, and that this report is best interpreted as a survey of *sensitivities* in each of the categories of mass reconstruction, cross sections, branching ratios, decay dynamics, and rare decays. In the event that this very massive fermion harbors surprises, this study benchmarks the capability to explore the new physics at the Tevatron facility.

Measurement	1 fb^{-1}	10 fb^{-1}	100 fb^{-1}	Comment
Yields				
N_{3jet*b}	580	5.8K	58K	*identified* events
$N_{4jet*2b}$	260	2.6K	26K	best m_t sample
δm_t	3.5	2.0	??	total precision GeV/c^2
Production				
$\delta\sigma_{t\bar{t}}$	11%	6%	5%	test top QCD couplings
$\delta\sigma_{ll}/\sigma_{l+j}$	14%	4.8%	1.5%	test non W decay
$\delta\sigma_{t\bar{b}X+b\bar{t}X}$	26%	10%	7%	isolate "single top"
$\delta\sigma \cdot B(Z' \to t\bar{t})$	100 fb	25 fb	10 fb	"topcolor" $M_{Z'} = 1$ TeV/c^2
Decay				
$\delta B(t \to W(b))$	3%	1.0%	0.3%	from N(bb)/N(bX)
$\delta B(t \to b(W))$	10%	3.5%	1.0%	from N(ll)/N(lX)
$\delta B(W_{V+A})$	3%	0.8%	0.3%	$W \to l\nu$ helicity
$\delta B(W_{long})$	6%	2.1%	0.7%	$\frac{W_{long}}{W_{left}} = \frac{1}{2}(\frac{m_t}{m_W})^2$
$\delta\Gamma(t \to Wb)$	28%	12%	10%	using single top
δV_{tb}	14%	6%	5%	from above
Rare Decays				
$B(c\,\gamma)$	$\leq 3.0 \times 10^{-3}$	$\leq 4.0 \times 10^{-4}$	$\leq 8.4 \times 10^{-5}$	(95% CL)
B(cZ)	$\leq 1.5 \times 10^{-2}$	$\leq 3.8 \times 10^{-3}$	$\leq 6.3 \times 10^{-4}$	(95% CL)
B(Hb)	$\leq 15\%$	$\leq 6\%$	$\leq 2\%$	from σ_{ll}/σ_{l+j}

Table 3.22: A Top Physics Program: Summary of expected precision vs integrated luminosity at the Tevatron

Acknowledgements

Many people have helped in the organization and discussion leading up to this document. We gratefully acknowledge the assistance of A. Belyaev, A. Beretvas, E. Boos, J. Butler, D. Carlson, W. Cobau, D. Gerdes, J. Hylen, J. Incandela, J. Konigsberg, M. Kruse, S. Parke, T. Stelzer, P. Tipton, J. Wells, S. Willenbrock, W.M. Yao, and C.-P. Yuan.

P.B. would like to thank the Physics Department of U. Michigan for kind hospitality during his sabbatical leave from U. Kansas.

Bibliography

[1] F. Abe *et al.*(The CDF Collaboration), Phys. Rev. Lett. **74**, 2626 (1995).

[2] S. Abachi *et al.* (The DØ Collaboration), Phys. Rev. Lett. **74**, 2632 (1995).

[3] LEP Electroweak Working Group, LEPEWWG/95-02 (August 1995); P. H. Chankowski and S. Pokorski, Phys. Lett. **B356**, 307-312 (1995); J. Ellis, G.L. Fogli, and E. Lisi, hep-ph/9507424.

[4] T. LeCompte et al., "Extension of Central Muon Coverage for Run 2", CDF Note 3116 (April 1995).

[5] The CDF Collaboration, "Proposal for Run II Tracking System Upgrades for CDF", CDF Note 3079 (March 1995).

[6] We thank Mark Kruse for discussion of this point.

[7] The CDF B Tag Group, "A Generator Study of b Jets from TOP Decay", CDF Internal Note 2568 (May 1994).

[8] W. Cobau, private communication.

[9] E. Laenen, private communication.

[10] E. Laenen, J. Smith, and W.L. van Neerven, Phys. Lett. **B321**, 254 (1994).

[11] F. Abe et al., Phys. Rev. D. **50**, 2966 (1994).

[12] Qi Zhong Li-Demarteau, for the DØ Collaboration, at the Aspen Winter Conference (January 1996).

[13] M. Stronvink, in the Proceedings of the 10th Topical Workshop on Proton-Antiproton Collider Physics, Fermilab, DØ note 2611 (May 1995).

[14] S. Gruenendahl, for the DØ Collaboration, at the NLC Workshop, Stanford Linear Accelerator Center (February 1996).

[15] G. Marchesini and B.R.Weber, Nucl. Phys. **B310**, 461 (1988).

[16] F.A.Berends, W.T.Giele, H. Kuijf and B. Tausk, Nucl. Phys **B357**, 32 (1991).

[17] S. Vejcik, S.B. Kim, "Statistical Uncertainties for the Top Mass in Run 1B", CDF Note 2833 (September 1994).

[18] S.B. Kim and S. Vejcik, "Study of Gluon Radiation and Jet Energy Scale Using Z+jets and Photon + jets", CDF Note 3006 (February 1995).

[19] W. Yao, L. Galtieri, M. Garcia-Scrivers, and J. Lys, "Studies of Gluon Radiation Systematic Error with b-bbar Events and a Proposal of Multiple Underlying Events Correction on the Jet Energy", CDF Note 3257 (July 1995).

[20] S.B.Kim, S. Vejcik, and B. Harral, "Background Shapes of the Reconstructed Top Mass", CDF Internal Note 3007 (February 1995).

[21] R.H. Dalitz and G.R. Goldstein, Phys. Rev. D**45**, 1531 (1992).

[22] K. Kondo, Journal of the Physical Society of Japan, **57** 4126 (1988) and **60**, 836 (1991).

[23] U. Heintz, "Top Mass Analysis of Dilepton Events," DØ Note 2658 (July 1995).

[24] J. Cochran and U. Heintz, "A Measurement of Top quark Mass with Dilepton Events" DØ Note 2659 (August 1995).

[25] S. Snyder, to appear in the Proceedings of the European Physical Society Meeting, DØ Note 2836, (July 1995).

[26] P. Azzi *et al.*, "Evidence for $t\bar{t}$ Production in the All Hadronic Channel", CDF Note 3187 (June 1995).

[27] J. Incandela, "Using the B Decay Length Distribution in Top Events to Measure m_t", CDF Note 1921 (December 1992).

[28] L. Orr, T. Stelzer, and W.J. Stirling, Phys. Rev. D **52**, 124-132 (1995); Phys. Lett. **B354**, 442-446 (1995); L. Orr and W.J. Stirling, Phys. Rev. D **51**, 1077-1085 (1995); S. Mrenna and C.-P. Yuan, Phys. Rev. D. **46**, 1007-1021 (1992); Yu. L. Dokshitzer, V.A. Khoze and S.I. Troyan, Proceedings of the 6th International Conference on Physics in Collision, Singapore (1987); G. Marchesini and B.R. Webber, Nucl.Phys. **B330**, 261-283.

[29] C.T. Hill, Phys. Lett. **B345**, 483-489 (1995).

[30] P. Cho and E.H. Simmons, Phys. Rev. D **51**, 2360 (1995); D. Atwood, A. Kagan and T. Rizzo, Phys. Rev. D **52**, 6264-6270 (1995).

[31] K. Lane, Phys. Rev. D **52**, 1546-1555 (1995).

[32] C. T. Hill, Physics Lett. **B266**, 419 (1991).

[33] K. Lane and E. Eichten, Phys. Lett. **B222**, 274 (1989); K. Lane and M.V. Ramana, Phys. Rev. D **44**, 2678 (1991).

[34] C. Hill, R. Harris, private communication

[35] K. Tollefson, R. Hughes, P. Tipton, B. Winer, "Search for Resonances Decaying to $t\bar{t}$", CDF Note 3105 (1995).

[36] For any given theoretical model, there may be angular correlations that either increase or decrease the acceptance and therefore the 5σ lines will move up or down slightly.

[37] I. Bigi *et al.*, Phys Lett. **B181**, 157 (1986).

[38] For example, see G. Kane, C.-P. Yuan, and G. Ladinsky, Phys. Rev. D. **45**, 124 (1992); D. Atwood, A. Aeppli, and A. Soni, Phys. Rev. Lett. **69**, 2754 (1992); R.S. Chivukula, S.B. Selipsky, E.H. Simmons, Phys. Rev. Lett. **69**, 575 (1992); M. Peskin, talk presented at the Second International Workshop on Physics and Experiments at a Linear e+e- Collider, Waikoloa, HI (April 1993); M.Peskin and P. Zerwas, talks presented at the First International Workshop on Physics and Experiments at a Linear e+e- Collider, Saariselka, Finland (September 1991); D. Carlson, E. Malkawi, C.-P. Yuan, Phys. Lett. **B337**, 145 (1994).

[39] G. Kane, C.-P. Yuan, and G. Ladinsky, Phys. Rev. D. **45**, 124 (1992).

[40] K. Fujikawa and A. Yamada, Phys. Rev. Lett. **49**, 5890 (1994).

[41] M. Jezabek and J.H. Kuhn, Phys. Lett. **B329**, 317 (1994).

[42] E. Malkawi, C.-P. Yuan, Phys. Rev. D. **50**, 4462 (1994).

[43] E. Thorndike, "Rare B Decays from CLEO, with emphasis on $b \to s\gamma$", Proceedings of the XXVII International Conference on High Energy Physics, Glasgow, UK (July 1994).

[44] S. Parke, "Summary of Top Quark Physics", FERMILAB -Conf-94/322-T, and Proceedings of DPF'94, University of New Mexico, Albuquerque, NM (August 1994).

[45] C. Couyoumtzelis, J. Conway, and A. Clark, private communication.

[46] S. Dawson, Nucl. Phys. **B249**, 42 (1985); S.S.D. Willenbrock and D.A. Dicus, Phys. Rev. D **34**, 155 (1986); S. Dawson and S.S.D. Willenbrock, Nucl. Phys. **B284**, 449 (1987); C.-P. Yuan, Phys. Rev. D **41**, 42 (1990); S. Cortese and R. Petronzio, Phys. Lett. **B253**, 494 (1991); G.V. Jikia and S.R. Slabospitsky, Phys. Lett. **B295**, 136 (1992), R.K. Ellis and S. Parke, Phys. Rev. D **46**, 3785 (1992); G. Bordes and B. van Eijk, Z. Phys. **C57**, 81 (1993); G. Bordes and B. van Eijk, Nucl. Phys. **B435**, 23 (1995).

[47] T. Moers, R. Priem, D. Rein and H. Reitler, in the Proceedings of the Large Hadron Collider Workshop, Aachen, 418 (1990).

[48] D.O. Carlson and C.-P. Yuan, Phys. Lett. **B306**, 386 (1993).

[49] A.P. Heinson, A.S. Belyaev and E.E. Boos, "Electroweak top quark production at the Fermilab Tevatron", in the proceedings of the Workshop on Physics of the Top Quark, Iowa State University, Ames, Iowa (May 1995), hep-ph/9509274.

[50] F.I. Olness and W.-K. Tung, Nucl. Phys. **B308**, 813 (1988).

[51] J. Botts, J.G. Morfin, J.F. Owens, J. Qiu, W.-K. Tung and H. Weerts, (CTEQ Collaboration) Phys. Lett. **B304**, 159 (1993).

[52] "The DØ Upgrade" by the DØ Collaboration, presented to the Fermilab PAC (April 1995).

[53] The electron efficiency in the DØ central calorimeter is 79.2%, and in the end calorimeters it is 63.1% [RECO V11.19, P. Grudberg, DØ Note 2316 (1994)].

[54] S. Chopra and R. Raja, DØ Note 2098 (April 1994).

[55] A.P. Heinson, A.S. Belyaev and E.E. Boos, "Single top quarks at the Fermilab Tevatron", in preparation.

[56] A.P. Heinson, DØ Note 2777 (1995).

[57] H. Weerts, private communication.

[58] T. Stelzer and S. Willenbrock, Phys. Lett. **B357**, 125-130 (1995).

[59] We thank S. Parke for discussion on this point.

[60] K. Fuji, "Top Physics at Future e^+e^- Colliders, Experimental Aspects", First International Workshop on Physics and Experiments at a Linear e+e- Collider, Saariselka, Finland (September 1991).

[61] G. Bagliesi *et al.*, *ibid.*

[62] M. Peskin *et al.*, *ibid.*

[63] P. Igo-Kemenes, M. Martinez, R. Miquel, and S. Orteau in Second International Workshop on Physics and Experiments at a Linear e+e- Collider, Waikoloa, HI (April 1993).

[64] P. Igo-Kemenes, *ibid.*

[65] D. Treille, *ibid.*

[66] G.A. Ladinsky and C.-P. Yuan, *ibid.*

[67] See for example D. Froidevaux, Top Quark Physics at LHC/SSC CERN/PPE/93-148 and Proceedings of Moriond 1993: Electroweak: 509-526 (March 1993).